Large-volume, helicon-plasma source for simulation experiments of space plasmas

Takao Tanikawa, Shunjiro Shinohara

Large-Volume, Helicon-Plasma Source for Simulation Experiments of Space Plasmas

Takao Tanikawa
Research Institute of Science and Technology, Tokai University,
Shibuya-ku, Tokyo 151-8677, Japan

Shunjiro Shinohara
Interdisciplinary Graduate School of Engineering Sciences,
Kyushu University, Kasuga, Fukuoka 816-8580, Japan

Abstract

A large-volume, helicon-plasma source (73.8 cm in diameter and 486 cm in axial length) has been developed to be used to investigate various wave phenomena observed in space plasmas, and its characteristics have been investigated. The discharge antenna used is a flat spiral type installed just outside the quartz-glass window at one end of the vacuum vessel, where the background magnetic field (B-field) is nonuniform. Antennae of two different sizes are used: 23 cm in diameter with 6 spiral turns and 43 cm in diameter with 4 spiral turns (the number of spiral turns is smaller for the latter so as not to increase the antenna inductance significantly). The uniform B-field in the central plasma region can be varied up to 2 kG. The plasma density after the density jump for Ar and He plasmas can exceed 10^{12} cm^{-3} with approximately 600 W of the injected rf power at 7 MHz. The reason for this excellent discharge efficiency is discussed, considering the power balance between input and loss. It has been found that the radial density profile can be varied rather easily by applying the following two means: 1) by changing the B-field configurations near the antenna by adjusting the field strength of the auxiliary coil installed near the antenna and 2) by changing the antenna radiation-field patterns by using the different rf feeding points on the antenna. By changing the magnetic field configuration near the antenna, the threshold power and the degree of the density change in a density jump can be varied. The electron density reaches the maximum away from the antenna; then decays weakly along the axial direction.

I. INTRODUCTION

Developing a large volume plasma source capable of producing high-density, current-free plasma is very important for many fields; as well, profile control under various magnetic field configurations is much needed. A helicon plasma source[1-10] that employs helicon waves for plasma production has been extensively investigated as a very efficient source of current-free dense plasma for both fundamental research and numerous application studies; e.g., plasma processing, nuclear fusion, and basic fields including space plasmas. Recently, an application to a magnetoplasma rocket[11] that would utilize this source was also proposed. Here, the helicon wave is a bounded electromagnetic wave in the whistler wave range of frequencies.

In spite of the extensive studies, most helicon sources are small, typically less than 10 cm in diameter, and use various kinds of antennae such as loop, helical, and saddle types wound around the outer side of the insulated tube (e.g., see Fig. 5 in Ref. 7), in straight magnetic field configurations. In addition, in small tube experiments, radial density profile control has not been successfully attempted in spite of it being recognized that this control is a critical problem that remains to be solved. Large helicon sources have been developed at some institutions and are summarized in Table 1[12-23] (from top to bottom, the device diameter becomes smaller). Although some machine sizes are relatively large, the actual diameter of the produced plasma column determined by the antenna geometry (see remarks regarding an antenna diameter that is close to the plasma diameter in Table I) is smaller than the device diameter. Three machines at Australian National,[19] Ruhr,[21] and West Virginia[22,23] Universities consist of two sections: a helicon plasma source and a diffusion chamber with the weaker magnetic field and the lower-density plasma. Contrarily, the machines used in the present study[12] and a previous one at Kyushu University[13,14] using spiral antennae installed at

just outside the vacuum chamber are quite different, in that the diameter of the plasma column can be as large as the device diameter itself by, e.g., simply increasing the antenna diameter. Here, several advantages to use a spiral antenna are described in Ref. 12.

In this paper, we present the characteristics of a very efficient, large-volume helicon plasma source (75 cm in diameter and 486 cm in axial length) at the Institute of Space and Astronautical Science (ISAS), which is a part of the Japan Aerospace Exploration Agency (JAXA). For this new device, we have again employed a spiral antenna scheme, aiming to produce large helicon plasma, whose volume is up to 2.1 m^3, with high efficiency: dependences of the electron density on various parameters, such as the rf input power, the fill pressure, and the magnetic field, have been carefully investigated. As well, innovative methods of controlling plasma profiles were demonstrated by changing the magnetic field configurations (varying the ratio of the field strength near the antenna to that in the mid-plane) and by changing the antenna radiation-field patterns. Our spiral antenna has several electrical terminals along the spiral tubes, so that any two terminals can be used to feed the rf power; in this way, the antenna radiation-field pattern as well as the capacitive effect can be easily varied. Developing easy ways to control the density profile is crucial in many plasma fields. Therefore, our large source with the capability of controlling the plasma profile can be expected to extend opportunities for plasma processing with a large-diameter, high density plasma in a low fill pressure condition; and assist in fundamental studies of plasmas relevant to space and fusion applications that inevitably require large volumes.

This report is organized as follows. Section II describes our experimental setup to produce large volume plasma using two types of spiral antenna. In Sec. III, we present various experimental results with some discussion, for example, the electron density profile as a function of input rf power and the efficiency of the plasma production. The control of the radial density profile by varying magnetic field configurations and antenna field patterns is

also demonstrated. Finally, in Sec. IV, the results are summarized.

II. EXPERIMENTAL SETUP

Figure 1 shows a schematic view of the large-volume helicon plasma source at ISAS/JAXA. A detailed description of this device including the rf system is in Ref. 12. The dimensions of the vacuum chamber are: 75 cm and 73.8 cm in outer diameter (o.d.) and inner diameter (i.d.), respectively, and 486 cm in axial length. Fourteen main field coils produce a uniform magnetic field in the central region of over 2 m extent along the axial direction (see Fig. 2), where the main coil current of I_m = 50 A generates a field strength of 140 G. Due to the absence of coils at either end of the machine, the magnetic fields in these regions become weaker and nonuniform. To compensate for the weak magnetic field near the spiral antenna located at one end of the chamber, additional coils are separately installed (right side in Fig. 1), and an independent power supply is used for them. Here, the three different values of the separate coil currents, I_s = 0, 10 and 20 A, correspond to the axial magnetic field near the antenna B_a = 11 G, 30 G, and 50 G, respectively, with I_m = 50 A, as is shown in Fig. 2. We note that varying the separate coil current I_s does not significantly alter the strength of the main magnetic field B_m in the central region of the chamber generated mostly by I_m. It can be seen from Fig. 2 (a) to Fig. 2 (c) that increasing I_s makes the degree of divergence of the field near the z = 0 region weaker: the magnetic field near the antenna increases with I_s in comparison to the main field, but the main field is still larger than the field near the antenna. Here, the position z = 0 cm corresponds to the inner surface (vacuum side) of the quartz-glass window for the antenna. As will be described in Sec. III B, it is possible to control the radial density profile of plasma by changing the magnetic field profile near the antenna (through varying the separate coil current I_s). In our experiment, the base pressure of the machine is ~ 10^{-7} Torr by

using a turbomolecular pump with a pumping speed of 1800 l/s. The typical working gas introduced to the machine through a needle valve is argon (Ar) and the fill pressure P_{Ar} is 0.2 – 2 mTorr.

Next, the rf system used in our experiment is described. Spiral antennae of two different diameters are used; the smaller one (type A) has 6 turns with 23 cm o.d. and the larger one (type B) has 4 turns with 43 cm o.d. Each of them has taps for electrical connections at every half-spiral turn. Any two-connection points can be chosen to feed the rf power to the antenna; in this way the antenna radiation-field pattern can be varied quite easily. This provides a way to control the radial electron density profile as will be described in Sec. III B. Antenna vacuum resistances R_v of types A and B without plasma are both ~ 0.85 Ω, including feed lines in a match box, at a frequency of 7 MHz. In this case, the high-voltage rf feeding point and the ground connection are at the outside and the center of the antenna, respectively. Reversing the role of connection points changes the value of R_V by less than 10%. These antennae are located outside of the chamber in atmosphere through a quartz-glass window. The diameter and thickness of the quartz window used with the type A (type B) antenna are 30 cm (52 cm) and 1.6 cm (3 cm), respectively. The distance between the surfaces of the quartz-glass window and antenna is typically 0.5 – 1 cm.

A split tank circuit is employed in the impedance matching box. The forward and reflected rf power, P_{for} and P_{ref}, respectively, are monitored by using a directional coupler, and the rf input power P_{inp} to the plasma is defined as $P_{for} - P_{ref}$. Antenna rf current and the voltage are also measured. The output rf power supply is < 1 kW with a typical frequency of 7 MHz in this experiment, using either continuous or repetitive pulsed (the pulse duration is 40 ms with a duty cycle of 0.04) modes.

The spatial plasma parameters such as the electron density n_e and electron

temperature T_e, whose typical value is 3 - 5 eV, are measured by spatially scanning Langmuir probes. The excited rf wave field patterns are measured using one-turn magnetic probes. To record the visual appearance of visible light emissions from the plasma, ordinary digital cameras are placed just outside the observation windows (see Fig. 1).

III. EXPERIMENTAL RESULTS AND DISCUSSION

A. Highly efficient helicon plasma production

1. Characteristics of produced plasma

Here, we present the experimental results showing the highly efficient production of high-density plasma. Throughout the paper, unless denoted specifically, the full spiral turns with the high voltage (ground) feeding point being the outer side (center) of the antenna are used in a pulsed discharge mode. Figure 3 shows the relationships between the plasma densities n_e measured at three different axial locations, and the input rf power P_{inp}, changing the separate coil current I_s near the type A antenna. Plasma can be initiated at as low as $P_{inp} \sim$ 1 W, where n_e is on the order of 10^9 cm^{-3}. The discharge mechanism in this low density regime may be categorized as a capacitively coupled plasma (CCP) discharge.[6] In this regime of less than 10^{10} cm^{-3}, the antenna loading is worse than that in the higher density regimes of 10^{12} cm^{-3} by a factor of several times; as described later (see, e.g., Figs. 6 and 7 using the type B antenna), and thus the rf antenna voltage is relatively high (see also the discussion of Fig. 11 noting that the antenna rf high voltage is important to generate the plasma in a low power regime, which shows the CCP effect). Wave propagation along the z axis is not observed before the density jump, and as is often seen[24] with increasing rf power, plasma behavior alters from CCP to helicon plasma discharge (HP) through inductively coupled plasma ICP[6,25] The electron density n_e increases with the increase in P_{inp}. When P_{inp} exceeds the

threshold power P_{th}, that is in a range of 70 – 300 W, a so-called 'a density jump' to the order of 10^{12} cm^{-3} is observed, which is characterized by a steep increase in density Δn_e and is known as a mode transition from ICP to HP discharges. The value of P_{th} and the large density increment of Δn_e (and also the large increase in antenna loading, which will be shown later in Fig. 6) are dependent on the separate coil current I_s, i.e., the strength of the magnetic field near the antenna, as is shown in Fig. 4. It can be seen that both P_{th} and Δn_e increase as I_s is increased. Note that the densities just before and after the jump also increase with I_s. This behavior agrees with the results of earlier experiments[26] and numerical results[27] (P_{th} and Δn_e increase as the external uniform magnetic field), using an $m = 0$ loop antennae wound around a small glass tube, and also with recent numerical results[28] calculated for nearly the same conditions as the present experiments using a spiral antenna. A tendency is shown for P_{th} to decrease with the increase in Ar fill pressure P_{Ar} (see, e.g., Fig. 5).

Whereas wave propagation along the z axis is not observed before the density jump, as mentioned, we have verified, through the measurements of the wave dispersion relation, that the discharge mechanism after the jump is indeed based on helicon waves (see, e.g., ref. 7 showing the electron density as a function of the parallel wavelength) by monitoring the axial component of the rf magnetic field. The radial profile of the wave magnetic field can be fitted to the Bessel function of J_0, showing also the m (azimuthal mode number) = 0 helicon wave characteristics. The wave structure after the jump tends to be clearer with an increase in I_s.

The electron density as a function of the input rf power for the type B antenna case (Fig. 5) shows the same tendency as with the type A antenna; plasma can be produced at low rf power ($P_{inp} < 1$ W), and the behavior of the density jump with I_s is similar to the type A antenna case. Note that for $I_s = 0$ and 8 A in Fig. 5 (a), there are no data points between $P_{inp} =$ 80 W and 200 W. This is due to the fact that the sudden improvement of the antenna coupling

to the plasma after the jump moves the discharge operating region around $P_{inp} \sim P_{th}$ into the higher input power region, preventing the discharge region just near P_{th}. For both type A and B antennae, plasma production can be initiated with a power of < 1 W, regardless of the strength (0 - 1600 G) of the main magnetic field, and the field near the antenna generated by I_s, and a fill pressure (0.2 – 2 mTorr). Plasma production can also be initiated at a fill pressure over 2 mTorr, as long as the pumping condition is satisfied. The maximum density obtained so far is 2.5×10^{12} cm^{-3} by the use of the type B antenna, with P_{inp} = 549 W, P_{Ar} = 0.5 mTorr, I_m = 286 A (corresponding to a main field of 800 G), and I_s = 16 A. This value of the maximum density is only limited by the capability of our rf amplifier whose maximum output power is 1 kW. An even higher density should be able to be obtained with a more powerful rf amplifier. Needless to say, this maximum density can also be expected to be higher with an increase in P_{Ar}.

As for the antenna-plasma coupling, the total antenna loading resistance R_t, which is the sum of R_v (vacuum loading resistance) and R_p (plasma loading resistance), is nearly constant or decreases slightly with the increase in rf input power (and thus with the increase in density n_e) in the region before the density jump, as is shown in Fig. 6. Here, sometimes there is a hump (e.g., $P_{inp} \sim 10$ W in Fig. 6) in the region before the density jump. The value of R_t rises abruptly after the density jump; R_t becomes a factor of 3 – 10 larger than R_v (= 0.85 Ω), showing a very good coupling due to the high density. This means that up to ~ 90 % of the input rf power is absorbed by the plasma. The plasma loading of R_p was experimentally high, and the preliminary computation[28] shows a high plasma loading with more than several Ω due to the rf large magnetic flux generation by the spiral antenna (multi-turn is important compared to a single turn with only less than a few Ω). Contrarily, an earlier small source experiment showed a low antenna loading: e.g., R_p with 5 cm diameter plasma less than 2 Ω with R_v = 0.27 Ω for a helical antenna,[29] although the ratio of R_p to R_v was as high as 7 under

a high electron density of $n_e > 10^{13}$ cm^{-3}, which shows good coupling efficiency. Figure 7 shows the plasma density n_e measured at two axial locations as a function of the total antenna loading R_t. In a low density region of less than ~ 2×10^{11} cm^{-3}, e.g., before the density jump, there are two regions if one inspects closely, which shows the two-valued function like behavior; one is the lower electron density region between ~ 10^9 and ~ 10^{10} cm^{-3} (probably CCP discharge dominates), and the other is the higher one between ~ 10^{10} and ~ 10^{11} cm^{-3} (probably ICP discharge dominates). In each region, there is a tendency that n_e (R_t) slightly decreases with the increase in R_t (n_e), as can be also seen in Fig. 6 (and the slope before the hump in Fig. 6 corresponds to the boundary between the two regions). After the jump, as is in Fig. 7, R_t increases almost linearly with n_e.

Discharge characteristics using helium gas are quite similar those with argon: n_e ~ 10^{12} cm^{-3} with $P_{inp} > 500$ W for $I_m = 50$ A and $I_s = 0$ A with a He fill pressure of $P_{He} = 0.75$ mTorr, although it is difficult to initiate the plasma with $P_{He} < 0.3$ mTorr. However, with an introduction of electron supply using a small heated tungsten wire located near the antenna at $z = 35$ cm, plasma can be produced much easier with better reproducibility, and the operating pressure in the low pressure region becomes wider.

2. Discussion on production efficiency

Here, we discuss the highly efficient plasma production obtained in our experiments; high-density plasma of more than 10^{12} cm^{-3} with just a little power of less than several hundreds of W in the large plasma source. As can be seen in Table I, the production efficiency of N_e / P_{rf}, which shows the ratio of total number of electrons to input rf power, is very high in our machine. Note that these values in this table are estimated very roughly using some assumptions such as density profile, and they do not always show typical values due to the limitations of using published data. This ratio of N_e / P_{rf} also means the electron density

per unit rf power density, and it is proportional to the (kinetic) energy confinement time τ_e, as is shown below.

$$\tau_e = \frac{3}{2}\int n_e\, k\left(T_e + T_i\right)dV \,/\, P_{rf} \sim \frac{3}{2}\, k\, T_e\, (N_e / P_{rf}) \ . \qquad (1)$$

Here, k and T_i are the Boltzmann constant and the ion temperature, respectively, and $T_e >> T_i$ is assumed neglecting radiation loss. If we take $N_e / P_{rf} = 10^{13}$ (1/W) and $T_e = 4$ eV, τ_e becomes 9.6 μs, and in our present machine it becomes 0.96 ms using $N_e / P_{rf} = 10^{15}$ (1/W), as is in Table I. There may be a tendency that N_e / P_{rf} increases with increases in plasma diameter, device size, magnetic field, and fill pressure, although parameter dependencies are difficult to be derived within a limited set of data. Of course, in the case of smaller machines, especially with a small plasma diameter, this N_e / P_{rf} becomes lower than those listed in Table I: e.g., 5 cm diameter and 170 cm long plasma[29] with the main magnetic field B_m = 1 kG field and Ar fill pressure P_{Ar} = 0.6 mTorr showed ~ 10^{13} (1/W), 4.7 cm diameter and 165 cm long plasma[30] with B_m = 0.8 kG and P_{Ar} = 15 mTorr showed ~ 0.5×10^{13} (1/W), and 5.6 cm diameter and 100 cm long plasma[31] with B_m = 1 kG and P_{Ar} = a few to 20 mTorr showed ~ 10^{13} (1/W).

To see the parameter dependence of the production efficiency, we plot this N_e / P_{rf} in Table I as a function of a^2, including for these three small machines[29-31]: N_e/P_{rf} is roughly proportional to $(a^2)^{0.82}$, and thus $S^{0.82}$, as is shown in Fig. 8 (a: plasma radius, S: plasma cross section area). Although there is some scattering, the correlation coefficient, which is written in this figure, using this scaling is not bad, and if we exclude the cases of the three small machines[29-31] and the two large machines[13,14] using spiral antennae including the present one, it may be difficult to achieve such a tendency due to the small range of a^2 with some scattering. The rough estimation that N_e/P_{rf} is nearly proportional to a^2 instead of $(a^2)^{0.82}$ can be understood from the following discussion; note that the detailed estimation of the diffusion

including anomalous ones, individual experimental conditions, and plasma parameters is almost impossible even though there are some discussions, e.g., refs. 30, 32 - 34 on energy and particle transports.

Generally, the obtained plasma is determined from the balance between plasma loss and generation. First, we discuss the former, i.e., plasma diffusion, to derive the above scaling, assuming that the input power to the plasma is the same as the rf input power. The ratio of the plasma radius to the Larmor radius for argon ions is in the range of 11 - 70 (4 – 25) assuming an argon ion temperature of T_i = 0.026 eV (0.2 eV due to the anomalous heating if it exists) in the devices in Fig. 8. On the other hand, the typical value of $\omega_{ci}\,\tau_{in}$ ($\omega_{ci}\,\tau_{ie}$) is mostly in the range of 0.2 – 6 (0.7 - 8), where ω_{ci} and τ_{in} (τ_{ie}) are the ion cyclotron angular frequency and the ion-neutral collision time (the ion-electron Coulomb collision time), respectively. Here, collision frequencies were estimated from refs. 33, 35, and 36 with T_i = 0.026 eV, and $\omega_{ci}\,\tau_{in}$ ($\omega_{ci}\,\tau_{ie}$) is proportional to B_m/P_{Ar} ($B_m\,T_i\,/n_e$). From the above estimation, ions are mostly weakly magnetized because of the small values of $\omega_{ci}\,\tau_{in}$ and $\omega_{ci}\,\tau_{ie}$ in spite of Larmor radius being smaller than the plasma diameter. Therefore, ions are considered to diffuse radially outward with the diffusion coefficient D_i = k T_i / m_i ν_i (m_i: ion mass, ν_i: total ion collision frequency). This means that ion particle confinement is proportional to a^2/D_i.

Here, we assume that plasma energy is lost with the same flux as the ion flux, which is diffusing toward the sidewall, although electrons may have a higher diffusion coefficient along the field lines than ions. This consideration comes from the total particle fluxes for ions and electrons being the same due to the ambipolar condition, in which slower diffusion species determine the actual loss. Note that the ion (electron) confinement time across (along) the field is roughly estimated to be ~ 8 ms (> 0.01 ms) in our present machine using D_i = k T_i / m_i ν_i (D_e = k T_e / m_e ν_e) and T_i = 0.05 eV with the use of typical density profiles, and that

the typical transit time determined by L/C_s along the field is ~ 0.8 ms. Here, m_e, ν_e, C_s, and L show the electron mass, the total electron collision frequency (sum of the electron-neutral and the electron-ion Coulomb collision frequencies), the ion sound velocity, and the half axial length of the device, respectively. The particle confinement time τ_p, which is expected to be nearly in the same range as the above ion confinement time, is larger than the energy confinement time τ_e of ~ 1 ms from Eq. (1), as was mentioned, which is consistent with the general law of $\tau_p > \tau_e$. Then, from the power balance, P_{rf} is written using the ion flux density $D_i \nabla n$ (n: density) to the sidewall with the surface of (2 L) (2 π a) and the mean energy W as:

$$P_{rf} = (2 \pi a) (2 L) (D_i \nabla n) W . \quad (2)$$

Here, the radial electric field is neglected and W is the mean energy to produce an ion and electron pair,[37] which is the sum of 1) the difference between the plasma potential on the axis and the floating potential at the wall, 2) the ionization energy, 3) the excitation energy, and 4) the electron kinetic energy. If we use n as $n_s = f\, n_e$, where n_e is taken as the volume averaged electron density, f is a numerical factor, and n_s is the electron density in the sheath edge, and assuming Bessel function (J_0), the radial density profile, N_e/P_{rf} can be written as,

$$N_e / P_{rf} = a^2 / (4.8\, D_i\, W\, f) . \quad (3)$$

This shows that N_e/P_{rf} is proportional to the plasma cross section $S = \pi a^2$, which is nearly the same tendency as in Fig. 8. This equation also shows that N_e/P_{rf} is proportional to the total ion collision frequency ν_i, as D_i is inverse proportional to ν_i. It is difficult to have scaling due to limited data, mostly that T_i and f are not known in addition to the lack of P_{Ar}

and T_e in some machines, but N_e/P_{rf} scales roughly as $(a^2 \nu_i)^{0.63}$ with a correlation coefficient of 0.70 using the data in Fig. 8. Inserting typical values into this equation in our present machine, and assuming D_i = 6 (m^2/s), W = 70 eV, T_i = 0.05 eV and f = 0.2, this becomes ~ 3 $\times 10^{15}$ (1/W), slightly larger than ~ 10^{15} (1/W) experimentally obtained, which is listed in Table I. Since the real diffusion rate which is influenced by some instabilities is generally higher than the classical one which we used, the above estimation can explain the experimental results quite well.

Although the above discussion suggests that N_e/P_{rf} is roughly proportional to a^2 (to be exact, the index is smaller than one, i.e., 0.82, from the data in Fig. 8), there may be other scaling candidates; but they cannot be interpreted from a physical picture using a limited dataset; e.g., N_e / P_{rf} can be also scaled as $(a L)^{1.2}$ and $V^{0.75}$ (V: plasma volume) with good correlations from the data used to derive Fig. 8. The above scalings include the term of a, and excluding it does not lead to a scaling with good correlation. However, the use of the parameter aB does not have a good correlation with N_e/P_{rf}. Here, this parameter is considered to be a measure of the ratio of plasma radius to the ion Larmor radius and a measure of the square root of the radial diffusion time across the magnetic field if ions are well magnetized; which is not true in the present dataset.

On the other hand, if the plasma loss is determined by the axial one, the input power P_{rf} is balanced by the outgoing energy flux of $(2\pi a^2) W (n_s C_s)$ along the field lines in two directions, coming from the simple consideration that the particles escape with a Bohm velocity C_s near the sheath at both ends of the chamber. We then have the following relation for the production efficiency.

$$N_e / P_{rf} = L / W C_s f . \qquad (4)$$

For convenience, inserting f = 0.2, L = 2 m, and W = 70 eV into Eq. (4), N_e / P_{rf}

becomes ~ 3×10^{14} (1/W), which is somewhat higher than the typical data shown in Table I. However, this formula shows that N_e / P_{rf} scales with L but not with a, which is different from the scaling in Fig. 8, and cannot explain the dataset used in this figure with a good correlation. Needless to say, primitive global confinement scaling using L / C_s, which is a modification of the above discussion, cannot explain the data either: since the input power P_{rf} is balanced by the term of $n_e\, W V / (L / C_s)$, the ratio of N_e to P_{rf} is written as,

$$N_e / P_{rf} = L / W C_s . \tag{5}$$

This also shows that N_e / P_{rf} scales with L but not with a.

In the production term, which must be balanced by the loss term, the spiral antenna may exhibit a good performance; in fact, the plasma loading of R_p was experimentally high, and as mentioned the preliminary computation[28] shows a high plasma loading with more than several Ω due to the rf large magnetic flux generation by the spiral antenna, regardless of the density in the range of > 10^{11} cm^{-3}; and also shows effective plasma production in the plasma core instead of the plasma surface. However, when R_p / R_v is high, a further increase in R_p does not lead to higher production efficiency, since the coupling power coefficient to the plasma is written as $R_p / (R_v + R_p)$ and saturation is expected in the range of the high R_p / R_v value. As was described in Sec. III A.1, in our experiments up to ~ 90 % of the input rf power was absorbed by the plasma. Nevertheless, the production region is important, e.g., the plasma core instead of the plasma edge, for a consideration of the production efficiency.

It can be seen from the above discussions that by using a spiral antenna applied to a large size device, we can achieve a better confinement condition (roughly proportional to the plasma cross section) with good production efficiency for obtaining highly efficient plasma production; in fact, the global energy confinement time τ_e experimentally obtained was ~ 1 ms, as was discussed, which is comparable to the Bohm diffusion time (transit time) of ~ 0.8

ms expressed roughly as L/C_s, although Bohm scaling cannot be applied. This τ_e value is reasonable since it is smaller than the estimated particle confinement time.

B. Control of spatial plasma profile

Here, we present the results of the radial and axial plasma profiles under various conditions. First, control of the radial electron density profile has been attempted by changing the magnetic field configuration near the antenna, which can be achieved by varying the separate coil current I_s near the antenna, as well as by changing the antenna radiation-field pattern in two ways, which can be realized by selecting different combinations of two rf feeding points on the antenna. Here, control using the latter method gives variability of the profile by reconnecting the antenna configuration. Figure 9 shows the radial profiles of the electron density measured at z = 150 cm using the former method, i.e., the magnetic field effect, with the type B antenna. These profiles are taken before [Fig. 9 (a)] and after [Fig. 9 (b)] the density jumps; changing I_s with the constant main field of 140 G except for the case in Fig. 9 (a), which has no magnetic field ($I_m = I_s = 0$ A). As shown in Fig. 9 (a), in which CCP/ICP discharges are expected, the magnetized plasma column with n_e in the order of 10^{10} cm^{-3} has a rather broad radial density profile, and this profile becomes broader with the increase in I_s from 0 to 16 A: the full width at half maximum (FWHM) widens from 35 to 42 cm. In the case of no magnetic field, i.e., $I_m = I_s = 0$ A, the plasma is much more uniform along the radial direction (FWHM is ~ 60 cm), although the density is low ($< 6 \times 10^9$ cm^{-3}) at z = 150 cm due to the monotonic decrease in n_e in the axial direction [see Fig. 14 (a)]. After the density jump, the discharge mode changes to HP mode; the plasma column also has a broader radial density profile with the increase in I_s. This tendency is much clearer especially for low P_{Ar}: FWHM is 16 (40) cm with I_s = 50 A and I_s = 0 (16) A with P_{Ar} = 0.5 mTorr, while FWHM is 30 (33) cm with I_s = 50 A and I_s = 0 (16) A with P_{Ar} = 2 mTorr.

The broadening of the plasma column with I_s has also been confirmed via visual observations of plasma light emissions captured by the digital cameras through the three observation windows in Fig. 1 (see also photos in Fig. 2 of Ref. 12). It has also been confirmed from the plasma light that the visible region of the plasma column extends to the other end of the chamber along the axis in the presence of the axial magnetic field (see Figs. 13 and 14). The dependence, after the jump, of the radial profile on I_s (or the magnetic field strength near the type B antenna) can be understood as follows: the degree of field convergence from the antenna region to the main field region becomes weaker (that is, field uniformity improves near the antenna) as I_s is increased; as a result, the plasma flows (and also the plasma is generated in the wave excitation region) more naturally along the field line to make the radial density profile broader. Note that compared to ICP or CCP, whose discharge region is localized near the antenna, this region of HP discharge is more extended in the axial direction.

Considering the above discussions of the magnetic configurations, a much more peaked radial density profile can be realized with a larger main field strength; e.g., FWHM becomes narrower of 13 cm when with I_s = 16 A and I_m = 286 A (main field is 800 G) due to the strong convergent field with $n_e = 2.5 \times 10^{12}$ cm^{-3} (the highest density case mentioned in Sec. III A), P_{inp} = 549 W, and P_{Ar} = 0.5 mTorr. From the effect of the magnetic configuration, where the convergent field case is discussed, it will be possible to widen the plasma column further if the divergent field is applied near the antenna region. This will be a great advantage in that the diameters of a spiral antenna and a window can be much smaller than the diameter of the plasma column; meaning that a small diameter plasma source can be made quite easily and inexpensively. We emphasize here that a helicon wave can propagate along the field lines in both convergent and divergent magnetic field configurations.[38]

The second method to control the radial electron density profile is to vary the

radiation-field pattern of the antennae in two ways; one is to change the position and the number of the turns of the spiral antenna used to radiate the rf fields, and the other is to switch the positions of the high voltage and ground feeding points, which have been described in Sec. II. To test the effectiveness of the former technique to control the radial density profile, the results of the two experiments, in which the inner 2 spiral turns and the outer 2 spiral turns of the type B antenna are used to radiate the rf fields, are compared with each other in Fig. 10. The radial density profile for the case of the outer 2 turns is broader than that for the case of the inner 2 turns. The radial profile, especially for the case of the outer 2 turns, often exhibits a hollow shape as can be seen in Fig. 10. Before (after) the density jump, which corresponds to Fig. 10 (a) [Fig.10 (b)], i.e, in the ICP (helicon) regime, the values of the FWHM are 50 (41) cm and 45 (33) cm for the cases of the outer 2 turns and the inner 2 turns, respectively. On the other hand, FWHM is found to be 41 cm in Fig. 10 (b) without a hollow profile after the density jump when using the full 4 spiral turns of the type B antenna. This FWHM for the full 4 turns lies between the cases of the inner 2 turns and the outer 2 turns in Fig. 10 (b). In figure 10 (a) and (b), it is demonstrated that use of the outer 2 turns shows the broader radial profile than the inner 2 turns, although the absolute values of FWHM depend on the density regime, i.e., the input power [see Fig. 10 (a) and (b)]. With a fill pressure of 0.5 mTorr in this figure, the production efficiency N_e / P_{rf} for the case of the inner (outer) 2 turns is worse by a factor of ~ 2.5 than (is nearly the same as) the one using the full 4 turns due to the smaller central electron density normalized by the input rf power and the smaller plasma size (a little bit broader profile is compensated by a little bit smaller central electron density normalized by the input rf power). The influence of the antenna field pattern on the density profile is also shown using the small spiral antenna (type A antenna); e.g., the inner 3 turns exhibits the higher value of the electron density in the inner plasma region, i.e., within 18 cm in diameter, than the one with the outer 3 turns, whereas the density

in the outer region of the plasma is nearly the same between the two antenna configurations. Here, the inner (outer) 3 turns have a central density of 4×10^{11} cm^{-3} (3×10^{11} cm^{-3}) after the density jump with P_{inp} ~ 200 W, P_{Ar} is 2 mTorr, the main field is 140 G with the main coil current I_m = 50 A, and the separate coil current I_s is 15A. The antenna loading and the relationship between n_e and P_{th} under different antenna conditions using the large antenna (type B antenna) is described later (see also Fig. 12).

These different profiles reflect the antenna's variations of the radiation-field pattern. Even for the case of the outer 2 turns, in which the rf electric field near the central region (especially azimuthal component) is weaker than the outer region of the antenna, the excited radiation-field patterns in the main plasma appear to be similar to the ones for the case of the full 4 turns, as long as helicon waves are excited (see also a discussion in the next paragraph of the CCP effect). This conclusion is deduced from the fact that, 1) except for the central region, the plasma profile is nearly the same in the two cases, and 2) density jumps are clearly observed in both cases. However, for the case of the outer 2 turns, the wave with the higher radial mode number with m = 0 may have also been partly excited in addition to the fundamental mode. This needs to be investigated further. Contrarily, in the case of the inner 2 turns, the region in which helicon waves are excited is expected to be narrower (constricted) in the radial direction.

The second way to change the radial density profile is to switch the positions of the high voltage and ground feeding points, as is described. We also found that even when we used the same inner 2 spiral turns of the antenna for the rf radiation, the radial electron density profile showed a broader (and sometimes hollow) profile, as shown in Fig. 11 (a) and (b), if the high-voltage side of the rf input is connected to the outer position of the antenna and its center is grounded. This can be understood as being the result of the CCP generation effect, since a high voltage is also applied to the outer 2 turns if the high voltage feeding

position is the outer position in the 2 inner turns, even though there is no direct rf current in the outer 2 turns. However, as the rf power is increased, from Fig. 11 (a) to (c), the CCP effect fades out due to the contribution of inductive and helicon generation effects becoming important. Here then are two ways to control radial density profiles, i.e., changes of antenna turns and the high voltage and earth feeding points, as described; and the results of the type B antenna showing this more clearly than those of the type A antenna, mainly due to the larger size of the antenna.

The discharge behavior and the antenna loading are now described. Figure 12 shows the relationship between n_e measured at two different axial locations and P_{inp} under the three antenna-field radiation conditions using the type B antenna. From this figure, the threshold power P_{th} for the density jump does not change appreciably by varying the antenna conditions, i.e., the radiation-field pattern and the high voltage feeding point. Compared to the use of the full 4 turns under the same condition as in Fig. 12, such as the magnetic field configuration and argon fill pressure, n_e and R_p after the jump are small being less than 5×10^{11} cm^{-3} (3×10^{11} cm^{-3}) and less than 0.7 Ω (0.5 Ω), respectively, for the case of the outer (inner) 2 turns with the high-voltage side of the rf input connected to the outer position of the antenna. In comparing the antenna loading between the case that the high-voltage side of the rf input is connected to the central position, and the case the outer position of the antenna. For the former case, compared to the latter case, R_p is small before the density jump (< 0.1 Ω) due to the small effect of the rf high voltage feeding position (small CCP effect), but slightly larger (< 0.9 Ω) after the jump mainly due to the higher electron density (see n_e vs P_{inp} in Fig. 12).

Next, the features of the axial density profiles are described. Figure 13 shows an example of the profile with using the type A antenna. The electron density increases along the z axis and reaches a maximum value of 1.35×10^{12} cm^{-3} at z ~ 60 cm, then gradually decreases. Figure 14 shows the axial n_e profiles using the type B antenna, before and after the

density jumps, for the various cases. For the purely ICP case without a magnetic field (i.e., $I_m = I_s = 0$ A) as shown in Fig. 14 (a), plasma decays monotonically along the z axis. Here, the e-folding length of the density decay is 43 cm. On the other hand, with a background magnetic field, regardless of the magnetic field configuration and of the presence of density jumps or the discharge regimes, the electron density n_e increases along the z axis, and the maximum position of n_e in the axial direction lies between 60 cm and 150 cm, depending on conditions such as the fill pressure and the magnetic field geometry (degree of convergent field). From previous results,[13] in a straight field configuration, the maximum position lay at roughly 15 – 40 cm, and increased with a decrease in the fill pressure.

Plasma uniformity along the z axis is very good; the decay length after the maximum density position is typically > 100 cm, as shown in Figs. 13 and 14, which becomes longer with a decrease in fill pressure and an increase in the separate coil current I_s (weaker convergent field). The weaker decay from lowering fill pressure is consistent with previous results.[13] These features of axial distributions are also confirmed from the plasma light measurements, and can be understood by the collisions with neutral particles that are determined mainly by the fill pressure, and from the plasma flows along the magnetic field line. Therefore, considering the above results, in order to achieve a uniform plasma in the axial direction without having a low electron density, it is better to have conditions (roughly) of $I_m > 30$ A (main field is > 84 G) and $I_s > 10$ A, as the magnetic field.

IV. CONCLUSIONS

A high-density helicon plasma source with very large volume, 75 cm in diameter and 486 cm in axial length, has been developed and the detailed characteristics of this source have been investigated; demonstrating a highly efficient plasma production and the control of the

radial density profile. Using two types of large spiral antenna, an electron density of more than 10^{12} cm^{-3} has been successfully produced using less than several hundreds of watts of input radio-frequency power; showing an excellent discharge efficiency. This efficiency and its scaling law were discussed, considering the power balance and the radial diffusion; from which it is suggested that N_e / P_{rf} scales with a^2.

By changing the magnetic field configuration, especially near the antenna region, threshold power and the increment of the electron density in the density jump can be varied. Plasma extends in the axial direction with a maximum position of z = 60 – 150 cm; and weak density decay, with a length of > 1 m after the density peak, is observed. Control of the radial density profile has been successfully carried out, by varying the magnetic field configurations and the antenna field patterns by selecting the various electrical connections of the antenna taps; with the former method, increasing the ratio of the magnetic field near the antenna and to the field in the midplane for the convergent field case caused a broader radial density profile. With the latter method, the use of outer turns showed a broader radial density profile compared to that of the inner turns, and a capacitive effect was also found by changing the high-voltage side of the rf input.

ACKNOWLEDGMENTS

This experiment was carried out at ISAS/JAXA under a research collaboration program. Encouragement from Professor Y. Nakamura, Professor Y. Kawai, and Professor K. Oyama has been greatly appreciated. We would also like to thank S. Sato, I. Funaki, and K. Aihara for their help in carrying out the experiments. The research has been partially supported by the Grants-in-Aid for Scientific Research (B)(2) the contract #15340199 and #1435051 from the Japan Society for the Promotion of Science.

References

[1] R. W. Boswell: Phys. Lett. A **33**, 457 (1970).

[2] R. W. Boswell: Plasma Phys. Control. Fusion **26**, 1147 (1984).

[3] F. F. Chen: Plasma Phys. Control. Fusion **33**, 339 (1991).

[4] A. Komori, T. Shoji, K. Miyamoto, and Y. Kawai: Phys. Fluida B **3**, 893 (1991).

[5] T. Shoji, Y. Sakawa, S. Nakazawa, K. Kadota, and T. Sato: Plasma Sources Sci. Technol. **2**, 5 (1993).

[6] M. A. Lieberman and A. J. Lichtenberg, *Principles of Plasma Discharges and Materials Processing* (John Wiley & Sons, Inc., New York, 1994).

[7] S. Shinohara, Jpn. J. Appl. Phys. **36**, 4695 (1997), and references therein.

[8] R. W. Boswell and F. F. Chen, IEEE Trans. Plasma Sci. **25**, 1229 (1997), and references therein.

[9] F. F. Chen and R. W. Boswell, IEEE Trans. Plasma Sci. **25**, 1245 (1997), and references therein.

[10] S. Shinohara, J. Plasma Fusion Res. **78**, 5 (2002), and references therein [mostly in Japanese].

[11] F. R. Chang-Díaz, Trans. Fusion Technol. **35**, 87 (1999).

[12] S. Shinohara and T. Tanikawa, Rev. Sci. Instrum.**75**, 1941 (2004).

[13] S. Shinohara, S. Takechi, and Y. Kawai, Jpn. J. Appl. Phys. **35**, 4503 (1996).

[14] S. Shinohara, S. Takechi, N. Kaneda, and Y. Kawai, Plasma Phys. Control. Fusion **39**, 1479 (1997).

[15] C. Watts, Rev. Sci. Instrum. **75**, 1975 (2004).

[16] C. M. Franck, O. Grulke, and T. Klinger, Phys. Plasmas **9**, 3254 (2002).

[17] C. M. Franck, O. Grulke, and T. Klinger, Phys. Plasmas **10**, 323 (2003).

[18] G. R. Tynan, M. J. Burin, C. Holland, G. Antar, and P. H. Diamond, Plasma Phys. Control.

Fusion **46**, A373 (2004).

[19]J. Scharer, A. Degeling, G. Borg, and R. Boswell, Phys. Plasmas **9**, 3734 (2002).

[20]J. Hana and C. Watts, Phys. Plasmas **8**, 4251 (2001).

[21]M. Krämer, B. Lorenz, and B. Clarenbach, Plasma Sources Sci. Technol. **11**, A120 (2002).

[22]P. A. Keiter, E. E. Scime, and M. Balkey, Phys. Plasmas **4**, 2741 (1997).

[23]M. W. Balkey, R. Boivin, J. L. Kline, and E. E. Scime, Plasma Sources Sci. Techonol. **10**, 284 (2001).

[24]A. R. Ellingboe and R. Boswell, Phys. Plasmas **3**, 2797 (1996).

[25]J. Hopwood, Plasma Sources Sci. Technol. **1**, 109 (1992).

[26]S. Shinohara and K. Yonekura, Plasma Phys. Control. Fusion **42**, 41 (2000).

[27]S. Shinohara and K. P. Shamrai, Plasma Phys. Control. Fusion **42**, 865 (2000).

[28]K. P. Shamrai and S. Shinohara, private communication.

[29]S. Shinohara, Y. Miyauchi, and Y. Kawai, Plasma Phys. Control. Fusion **37**, 1015 (1995).

[30]I. S. Sudit and F. F. Chen, Plasma Sources Sci. Technol. **5**, 43 (1996).

[31]B. Clarenbach, B. Lorenz, M. Krämer, and N. Sadeghi, Plasma Sources Sci. Technol. **12**, 345 (2003).

[32]F. F. Chen, I. S. Sudit, and M. Light, Plasma Sources Sci. Technol. **5**, 173 (1996).

[33]F. F. Chen, Plasma Sources Sci. Technol. **7**, 458 (1998).

[34]Th. Enk and M. Krämer, Phys. Plasmas **7**, 4308 (2000).

[35]S. C. Brown, *Basic Data of Plasma Physics* (The MIT Press, Cambridge, 1967).

[36]D. L. Book, *NRL Plasma Fromulary* (Washington, D.C.: Naval Research Laboratory) NRL/PU/6790-02-450 (2002).

[37]C. Charles, R. W. Boswell, and M. A. Lieberman, Phys. Plasmas **10**, 891 (2003).

[38]S. Takechi and S. Shinohara, Jpn. J. Appl. Phys. **38**, L1278 (1999).

Figure Legends and Table Caption

TABLE. I. Comparison of machine parameters between various large helicon sources from different organizations. Rough estimations have been done as to the production efficiency N_e / P_{rf}, where N_e and P_{rf} are total number of electron density and input rf power, respectively.

FIG. 1. Schematic view of the large volume, helicon plasma source.

FIG. 2. Calculation of the magnetic field as a function of the axial direction z, changing the separate coil current I_s near the antenna, with the main field of 140 G (main coil current I_m = 50 A): I_s = (a) 0 A, (b) 10 A, and (c) 20 A.

FIG. 3. Relationship between the electron density n_e and the input rf power P_{inp}, changing the separate coil current I_s near the type A antenna: I_s = (a) 0 A, (b) 5 A, (c) 10 A and (c) 15 A. Here, a fill pressure of P_{Ar} = 2 mTorr and the main field is 140 G (main coil current I_m = 50 A). Open circles, closed triangles, and open boxes show measurements at z = 37 cm, 150 cm and 370 cm, respectively. Vertical dotted lines denote the threshold rf input power P_{th} for the density jump.

FIG. 4. Dependences of the electron density n_e and the threshold input power P_{th} (crosses) on the separate coil current I_s near the type A antenna. Here, a fill pressure of P_{Ar} = 2 mTorr and the main field is (a) 70 G and (b) 140 G with the main coil current I_m = 25 A and 50 A, respectively. Open (closed) symbols of circles, triangles, and boxes denote the density measurements just before (just after) the density jump at z = 37 cm, 150 cm and 370 cm, respectively.

FIG. 5. Relationship between the electron density n_e and the input power P_{inp} with a fill pressure of P_{Ar} = (a) 0.5 mTorr and (b) 2 mTorr. Here, the main field is 140 G with the main coil current I_m = 50 A. Open (closed) symbols of circles, triangles, and boxes show the measurements at z = 40 cm (150 cm), with the separate coil current I_s near the type B antenna of 0 A, 8 A, and 16A, respectively.

FIG. 6. Relationship between the total antenna loading R_t and the input power P_{inp} with a fill pressure of P_{Ar} = 2 mTorr and a main field of 140 G (the main coil current I_m = 50 A), for the same condition as that in Fig. 5 (b) using the type B antenna. The vacuum loading R_v is 0.85 Ω, and closed triangles (open boxes) show the case with the separate coil current I_s near the type B antenna of 8 A (16A).

FIG. 7. Relationship between the electron density n_e and the total antenna loading R_t with a fill pressure of P_{Ar} = 2 mTorr and the main field of 140 G (the main coil current I_m = 50 A), for the same condition as that in Fig. 5 (b) and Fig. 6, using the type B antenna. The vacuum loading R_v is 0.85 Ω, and open and closed triangles (open and closed boxes) show the case measured at z = 40 cm and 150 cm, respectively, with the separate coil current I_s near the type B antenna of 8 A (16A).

FIG. 8. Relationship between N_e / P_{rf} and a^2 using various machine data from Table I and three small devices.[29-31] Here, N_e, P_{rf}, and a show the total number of electrons, input rf power, and plasma radius, respectively. A least square fitting curve in the power series (broken line) and the correlation coefficient R with the fitting function on the top of the figure are also shown. Here, x (in unit of m^2) and y (in unit of 10^{13}/W) correspond to a^2 and N_e / P_{rf}, respectively.

FIG. 9. Radial profiles of the electron density n_e at z = 150 cm, changing the magnetic field configurations with the type B antenna and a fill pressure of P_{Ar} = 2 mTorr: (a) Open boxes, open triangles, and closed triangles show (I_m, I_s) = (0 A, 0 A), (50 A, 0 A), and (50 A, 16 A), respectively, where I_m is the main coil current and I_s is the separate coil current I_s. (b) Open and closed circles (open and closed triangles) mean (I_m, I_s) = (50 A, 0 A) and (50 A, 16 A), respectively, with a fill pressure of P_{Ar} = 0.5 (2) mTorr.

FIG. 10. Radial profiles of the electron density n_e at z = 150 cm, changing electrical connections of taps in the type B antenna with a fill pressure of P_{Ar} = 0.5 mTorr, the main coil current I_m = 50A, and the separate coil current I_s = 16 A: (a) Closed triangles and open boxes show the cases having outer 2 turns or inner 2 turns, respectively, before the density jumps, and (b) Open circles, closed triangles, and open boxes denote the cases of 4 full turns, outer 2 turns, and inner 2 turns, respectively, after the density jumps.

FIG. 11. Radial profiles of the electron density n_e at z = 150 cm, changing the electrical connections of the taps in the type B antenna (using inner 2 turns) with a fill pressure of P_{Ar} = 0.5 mTorr, the main coil current I_m = 50A, and the separate coil current I_s = 16 A. Here, closed triangles (open boxes) denote the high voltage-side of the rf input being at the outer side (inner side) of the antenna. The input rf power P_{inp} is increased from (a) to (c); cases (a) and (b) are taken before the density jumps, and case (c) is after the jumps.

FIG. 12. Relationship between the electron density n_e and the input power P_{inp} with a fill pressure of P_{Ar} = 0.5 mTorr for the same condition as that in Fig. 10, using the type B antenna. Here, the main field is 140 G with the main coil current I_m = 50 A and the separate coil current I_s near the type B antenna is 16A. Open (closed) symbols of circles, triangles, and boxes show the measurements at z = 40 cm (150 cm);using the outer 2 spiral turns with the

high-voltage side of the rf input connected to the outer position of the antenna, the inner 2 turns with the high-voltage side connected to the outer position, and the inner 2 turns with the high-voltage side connected to the inner position, respectively.

FIG. 13. Axial profiles of the electron density n_e using the type A antenna with a fill pressure of P_{Ar} = 2 mTorr, rf input power P_{inp} = 390 W, main coil current I_m = 50A, and separate coil current I_s = 15 A.

FIG. 14. Axial profiles of the electron density n_e using the type B antenna (a) before and (b) after the density jumps: (a) Open boxes, open triangles, and closed triangles show (I_m, I_s) = (0 A, 0 A), (50 A, 0 A), and (50 A, 16 A), respectively, where I_m is the main coil current and I_s is the separate coil current I_s. (b) Open and closed circles (open and closed triangles) denote (I_m, I_s) = (50 A, 0 A) and (50 A, 16 A), respectively, with a fill pressure P_{Ar} = 0.5 (2) mTorr.

Organization	**Machine Size** (Diameter, Length) in cm	**Maximum Field** (kG)	**Plasma Volume** (m^3)	Ne/P_{rf} in 10^{13} (1/W)	**Remarks**
ISAS/JAXA	(75, 486) (Present) (Ref. 12)	2	2.1	~ 100 (0.14 kG, 2 mTorr)	Nonuniform Field Spiral Antenna
Kyushu Univ.	(45, 170) (Refs. 13,14)	2	0.26	~ 30 (< 0.2 kG, 10 mTorr)	Spiral Antenna
New Mexico Tech.	(43, 400) (ALPHA) (Ref. 15)	2.2	0.053 each	~ 8 (0.8 kG, 3 mTorr)	Plasma Diameter: 13 cm each in Seven Sources
Max Planck Institute (Greifswald)	(40, 450) (VINETA) (Refs. 16, 17)	1	0.035	~ 2 (0.85 kG, 2 mTorr)	Plasma Diameter: 10cm
Univ. California, San Diego	(20, 250) (CSDX) (Ref. 18)	1	0.020	~ 4 (1 kG, 3 mTorr)	Plasma Diameter: 10cm
Australian National Univ.	(20, 50) + (90, 250) (WOMBAT) (Ref. 19)	0.1 + 0.06	0.016 + 1.6	~ 2 (0.1 kG, 3 mTorr)	
Auburn Univ.	(15, 250) (ALEPSI) (Ref. 20)	0.8	0.020	~ 5 (0.8 kG, 9 mTorr)	Plasma Diameter: 10 cm
Ruhr Univ.	(15, 200) + (60, 100) (Ref. 21)	1	0.034 + 0.28	~ 5 (< 1 kG)	Multipole Field in Large Diameter Chamber
West Virginia Univ.	(15, 157) (HELIX) + (200, 450) (LEIA) (Refs. 22, 23)	1.3 + 0.07	0.028 + 14	~ 5 (< 1 kG, 6 mTorr)	

Table I. S. Shinohara et al.

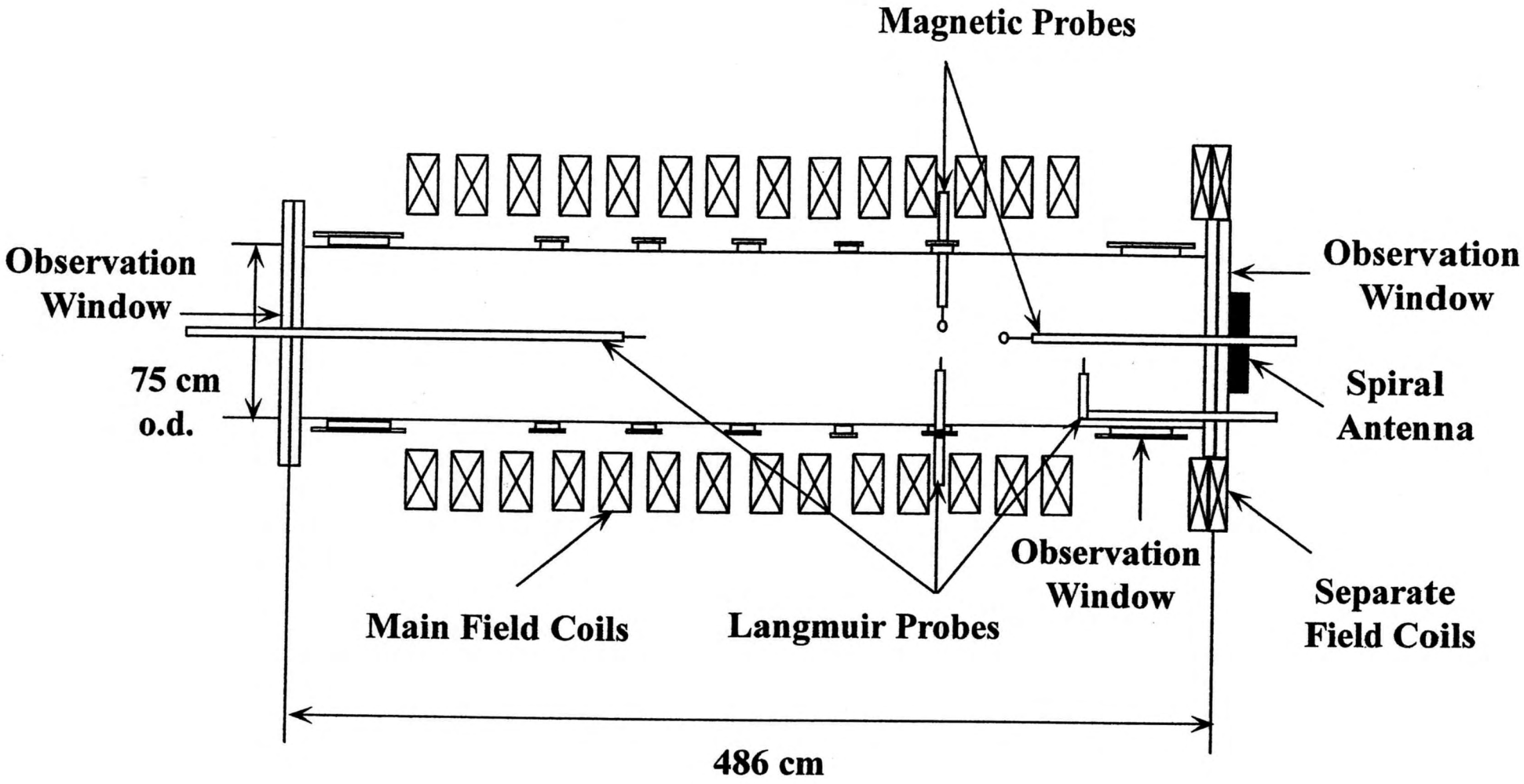

Fig. 1. S. Shinohara et al.

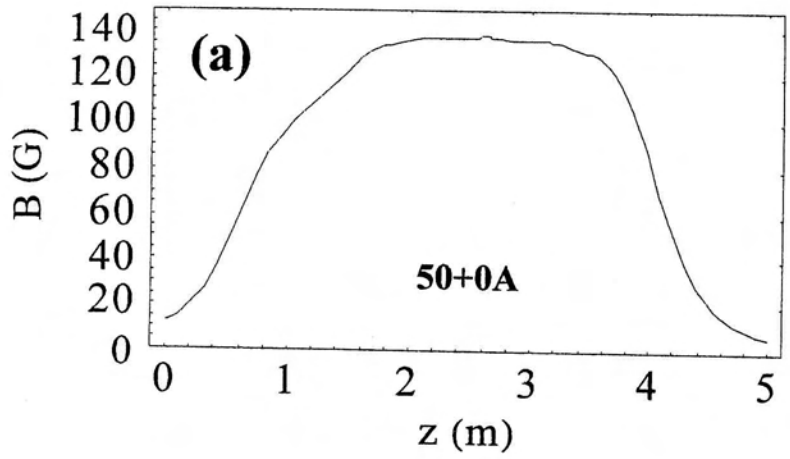

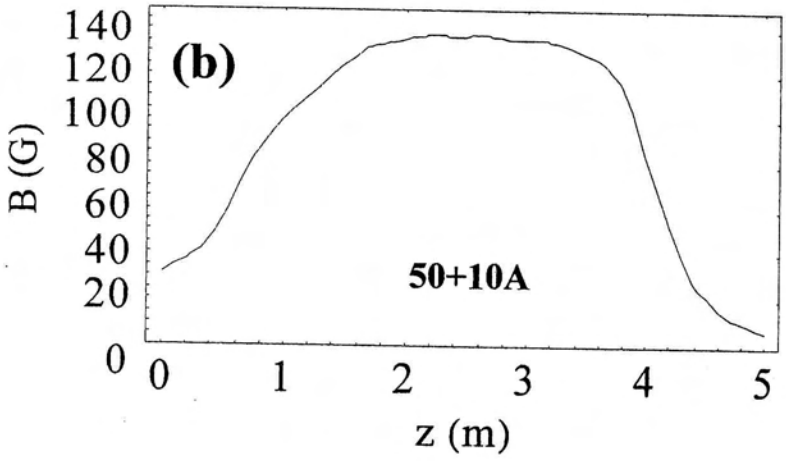

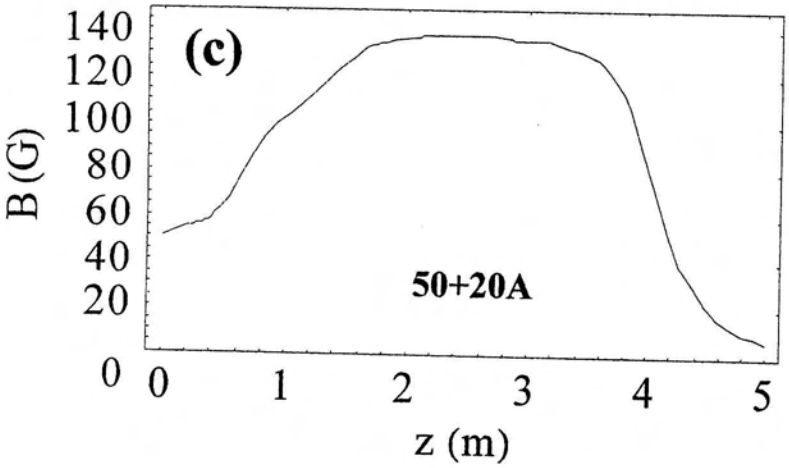

Fig. 2. S Hisatsune et al.

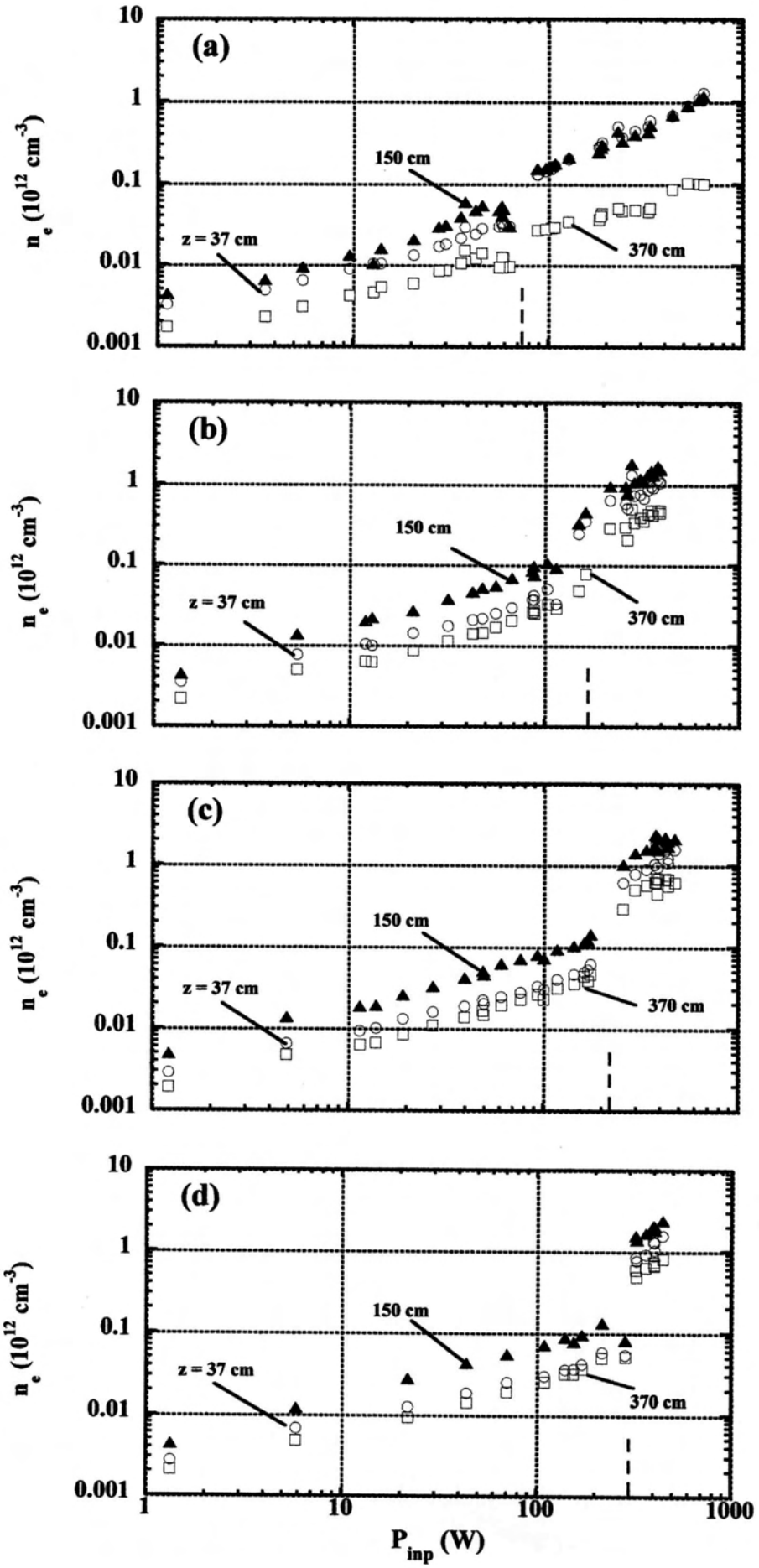

Fig. 3. S Shinohara et al.

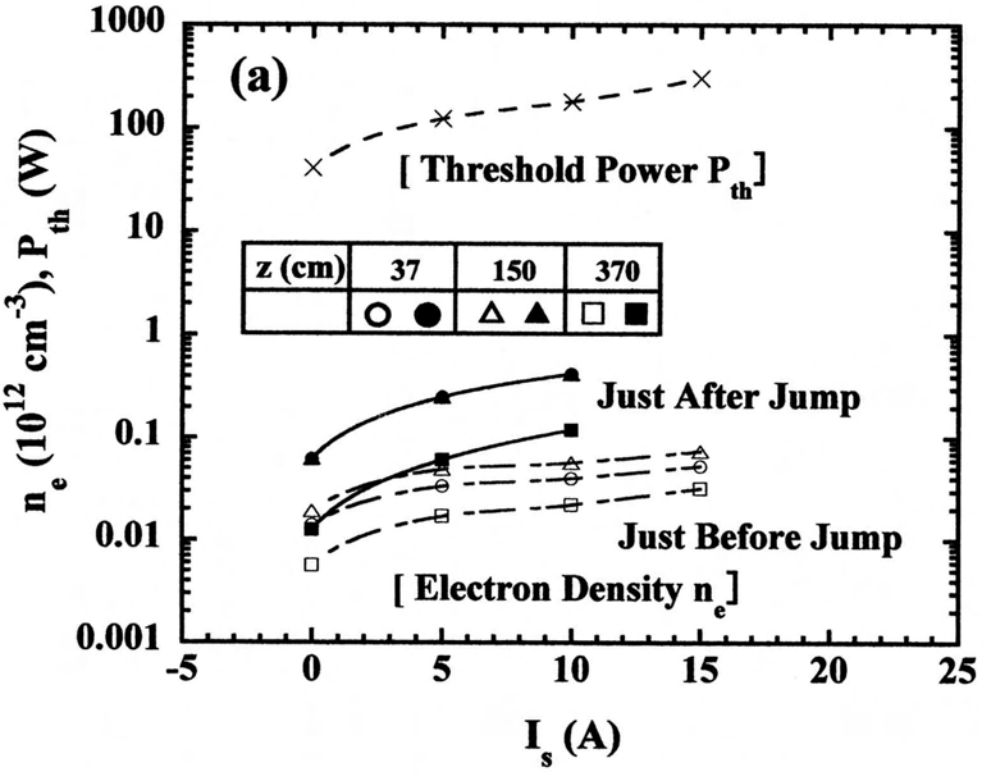

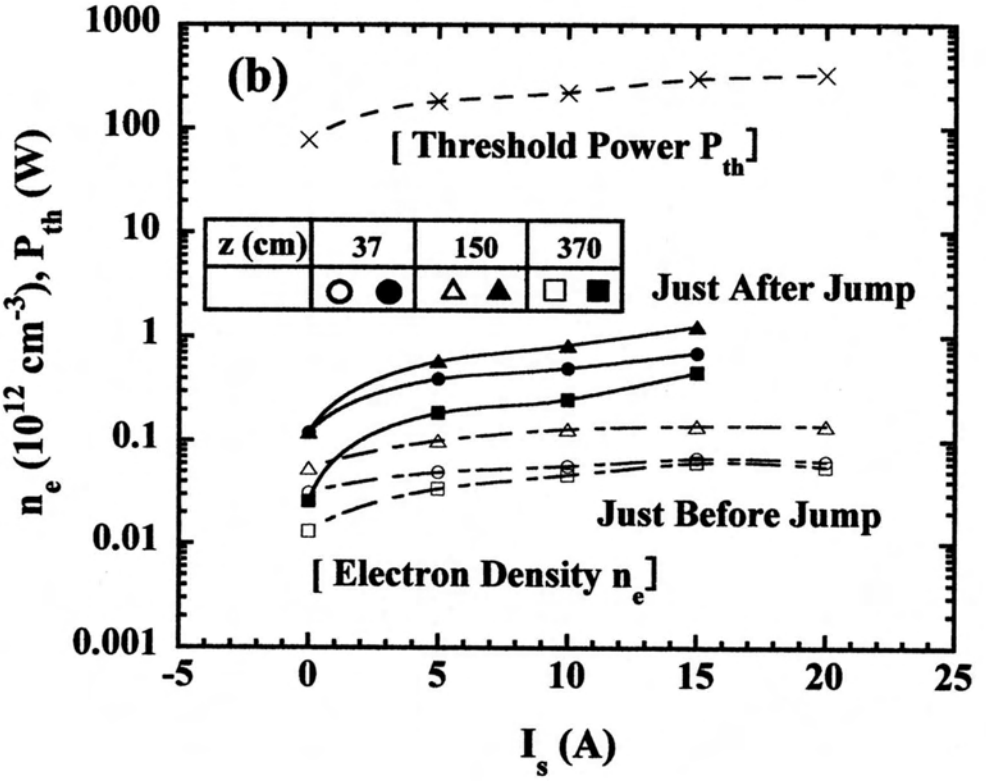

Fig. 4. S. Shinohara et al.

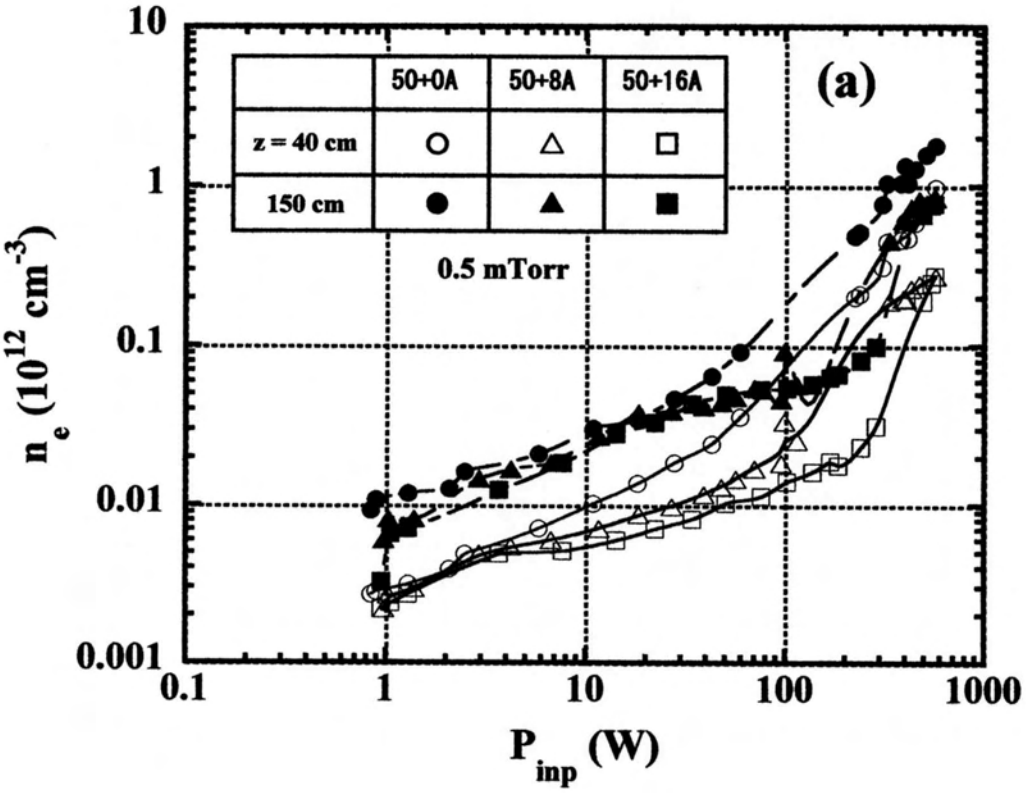

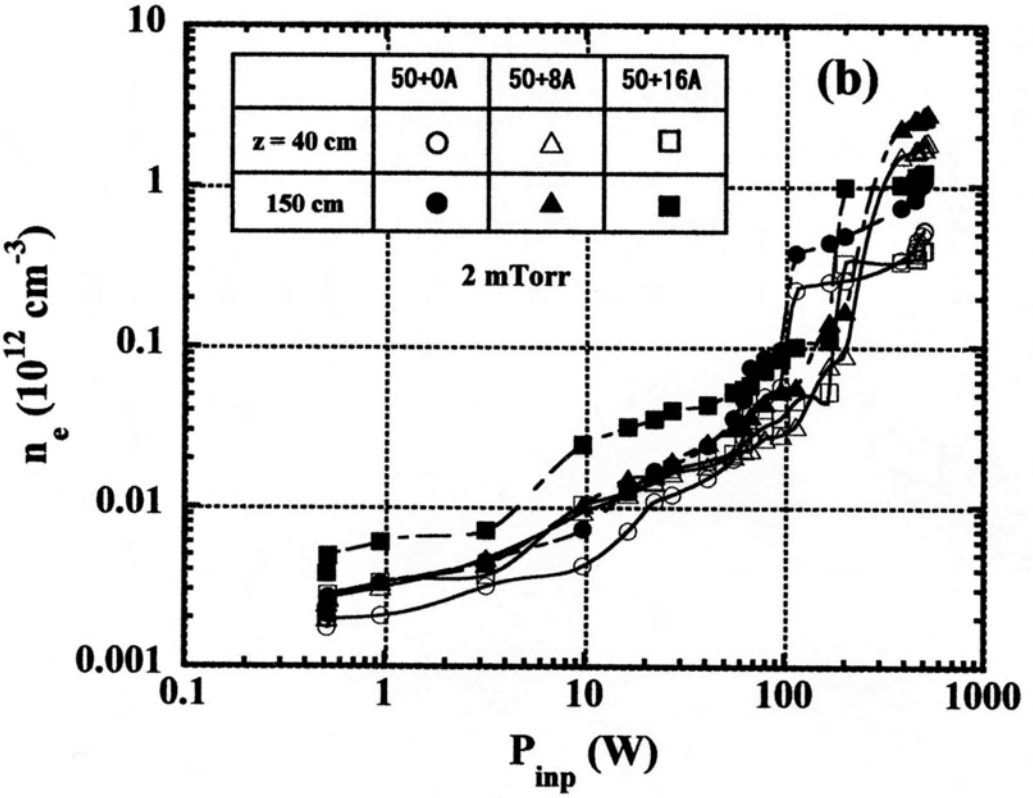

Fig. 5. S. Shinohara et al.

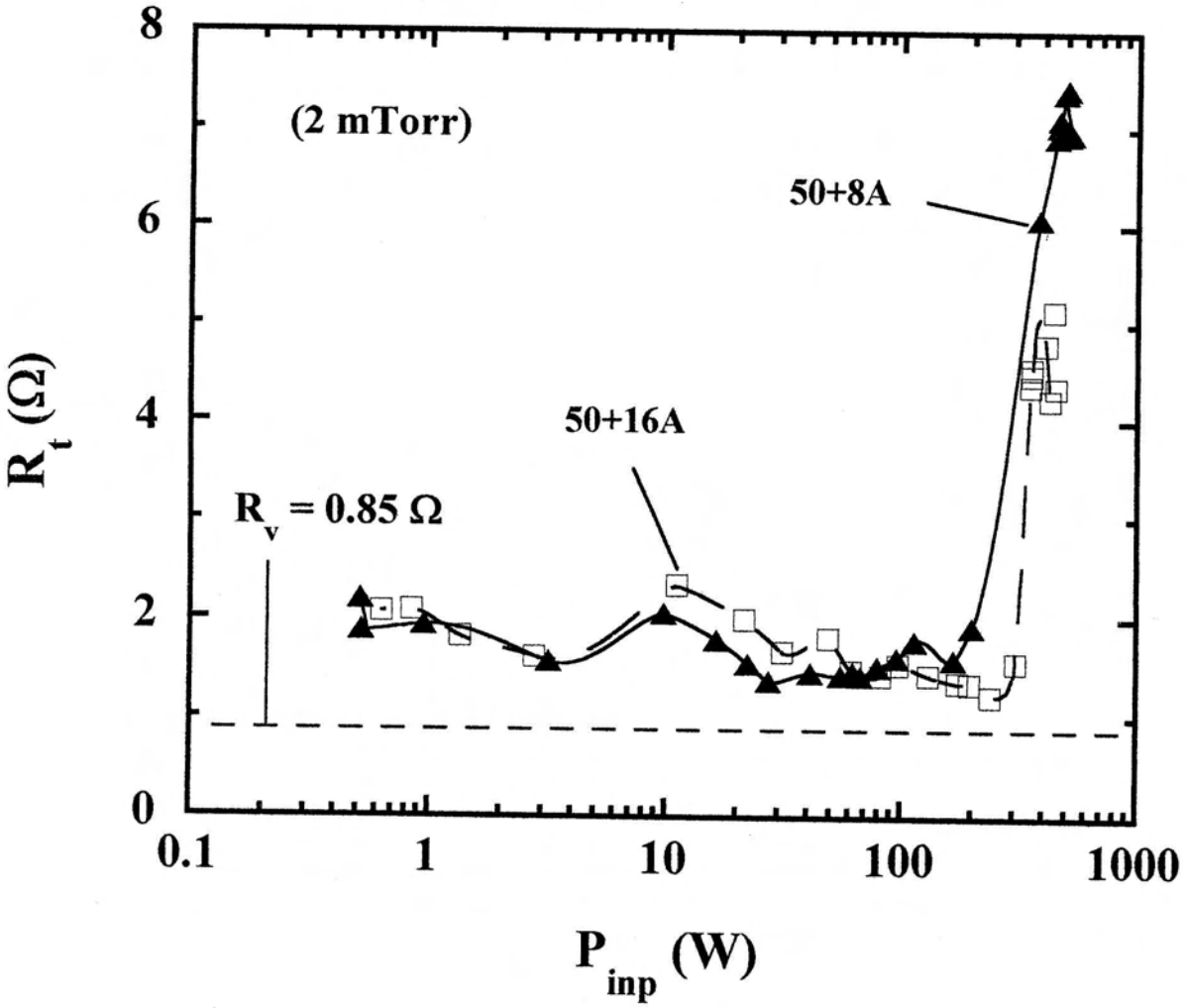

Fig. 6. S. Shinohara et al.

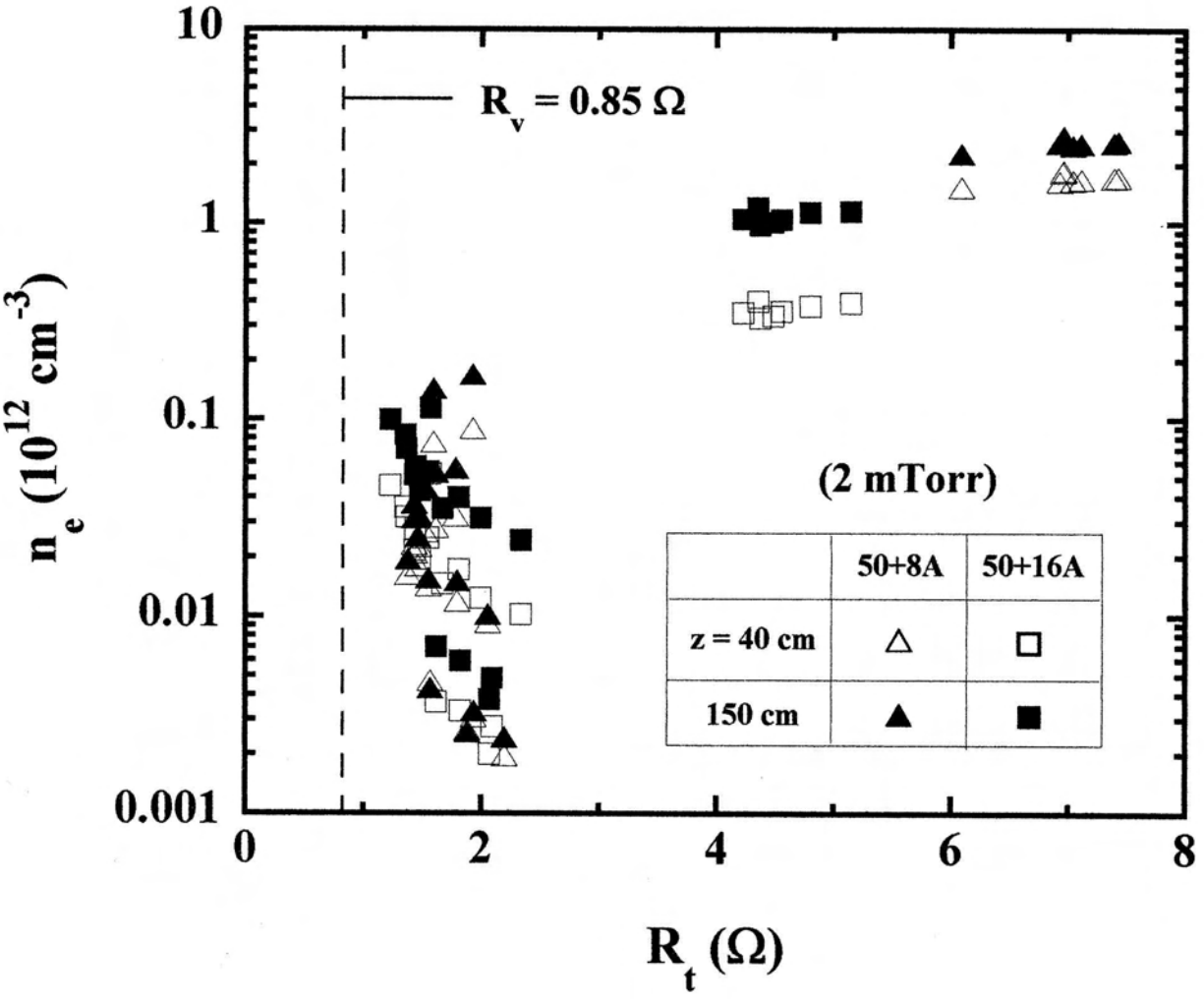

Fig. 7. S. Shinohara et al

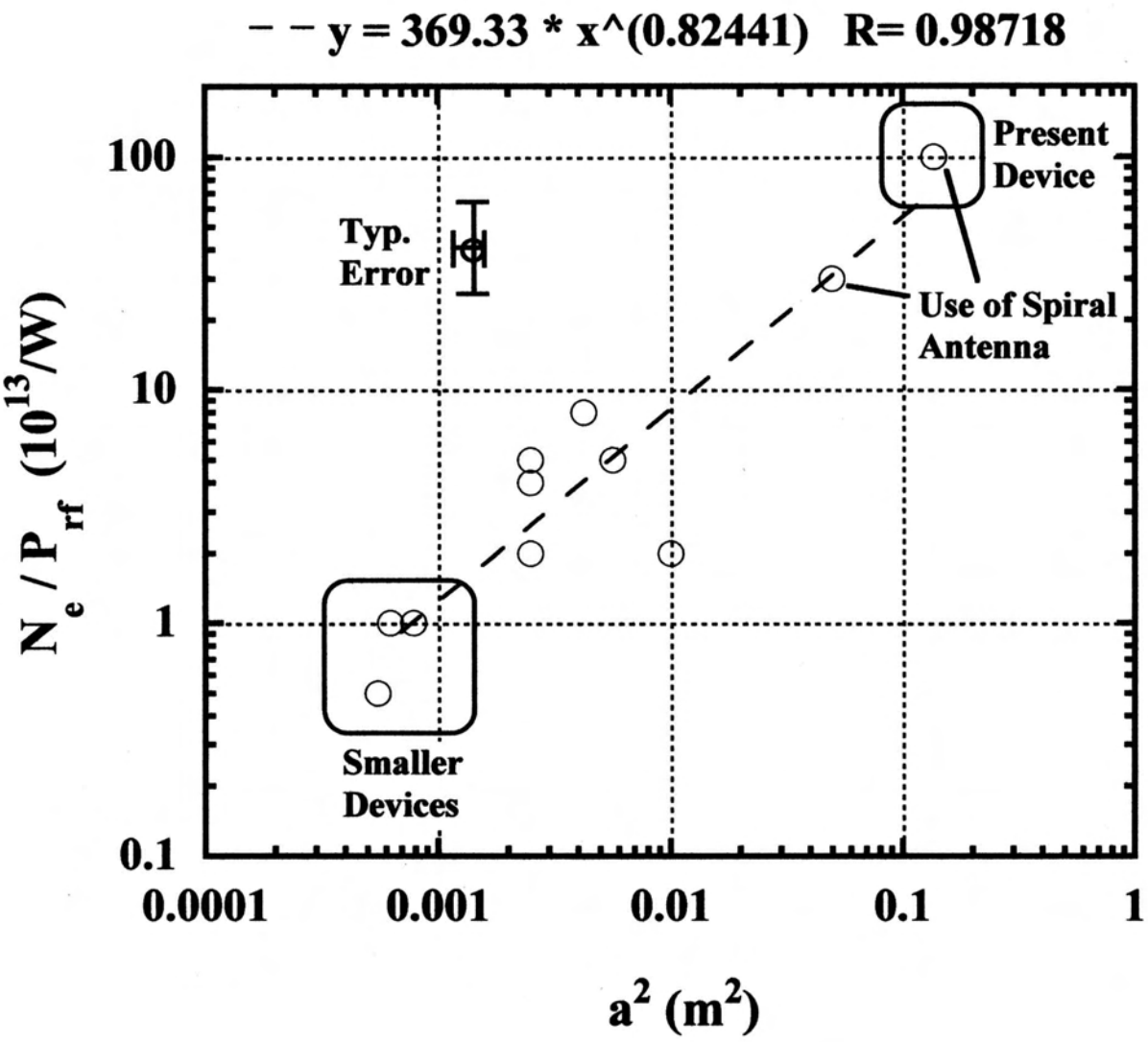

Fig. 8. S. Shinohara et al.

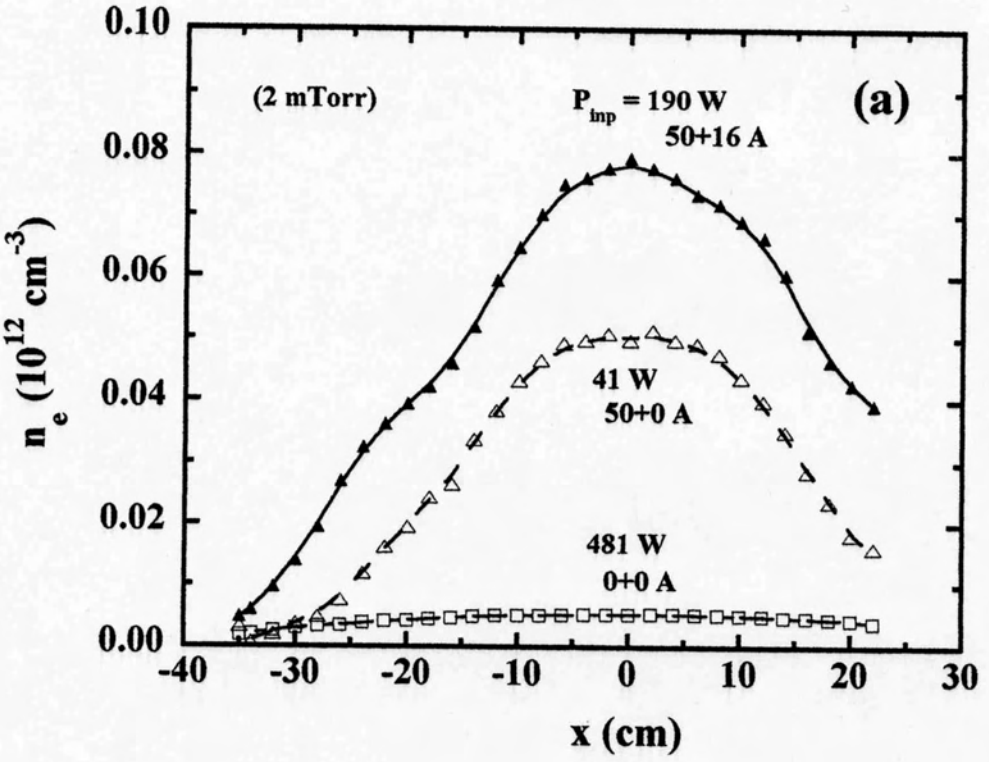

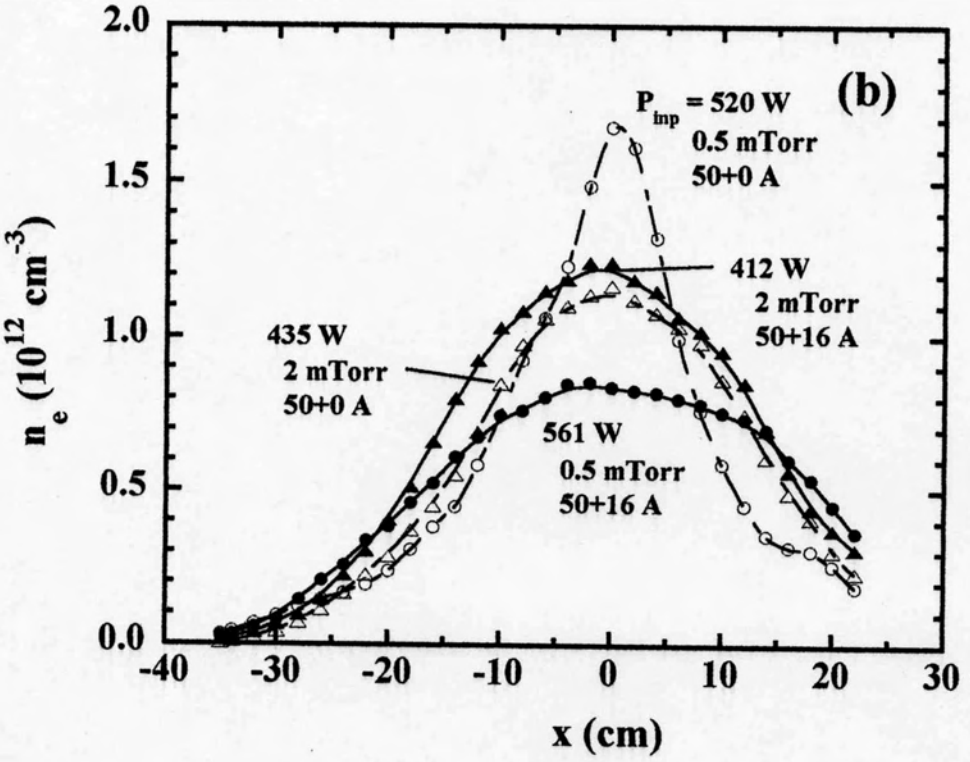

Fig. 9. S. Shinohara et al.

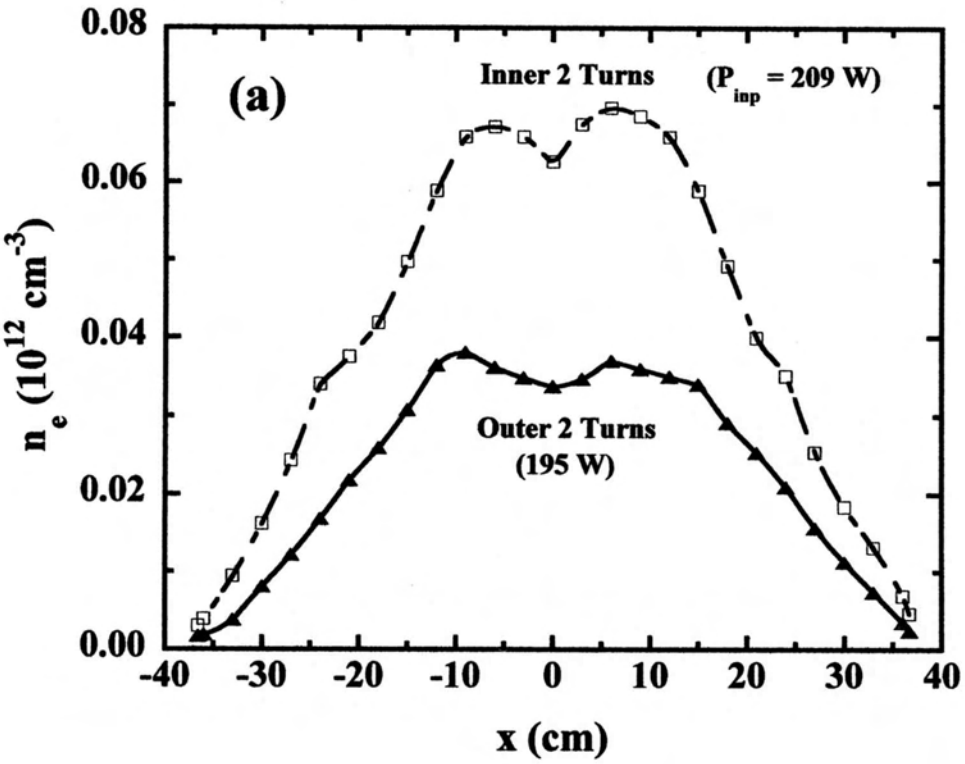

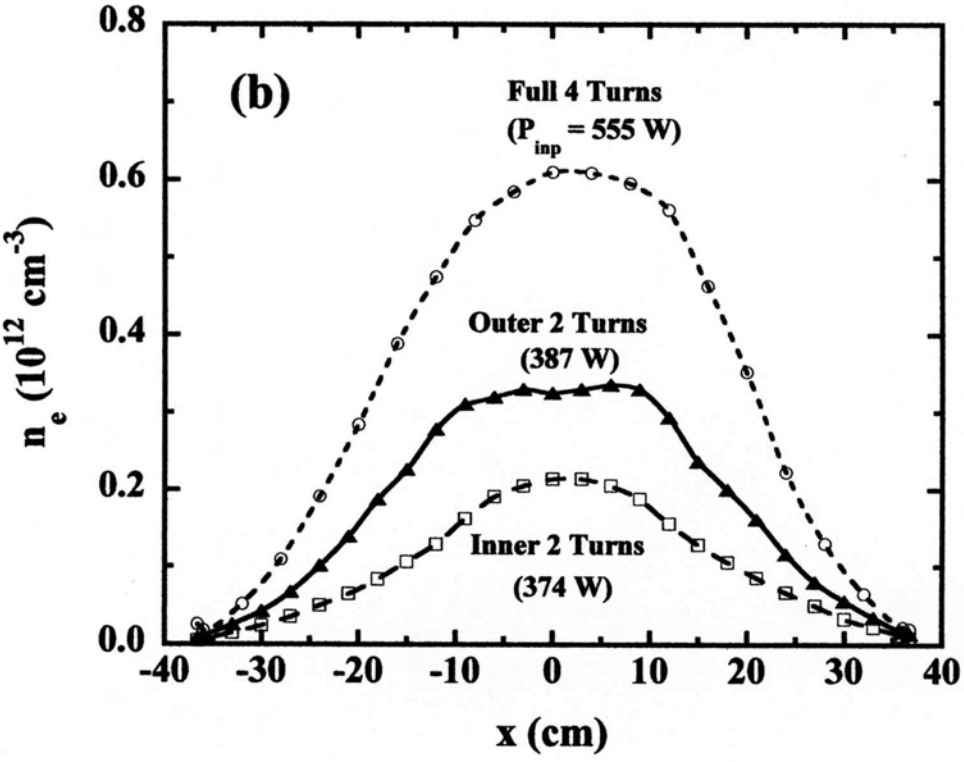

Fig. 10. S. Shinohara et al.

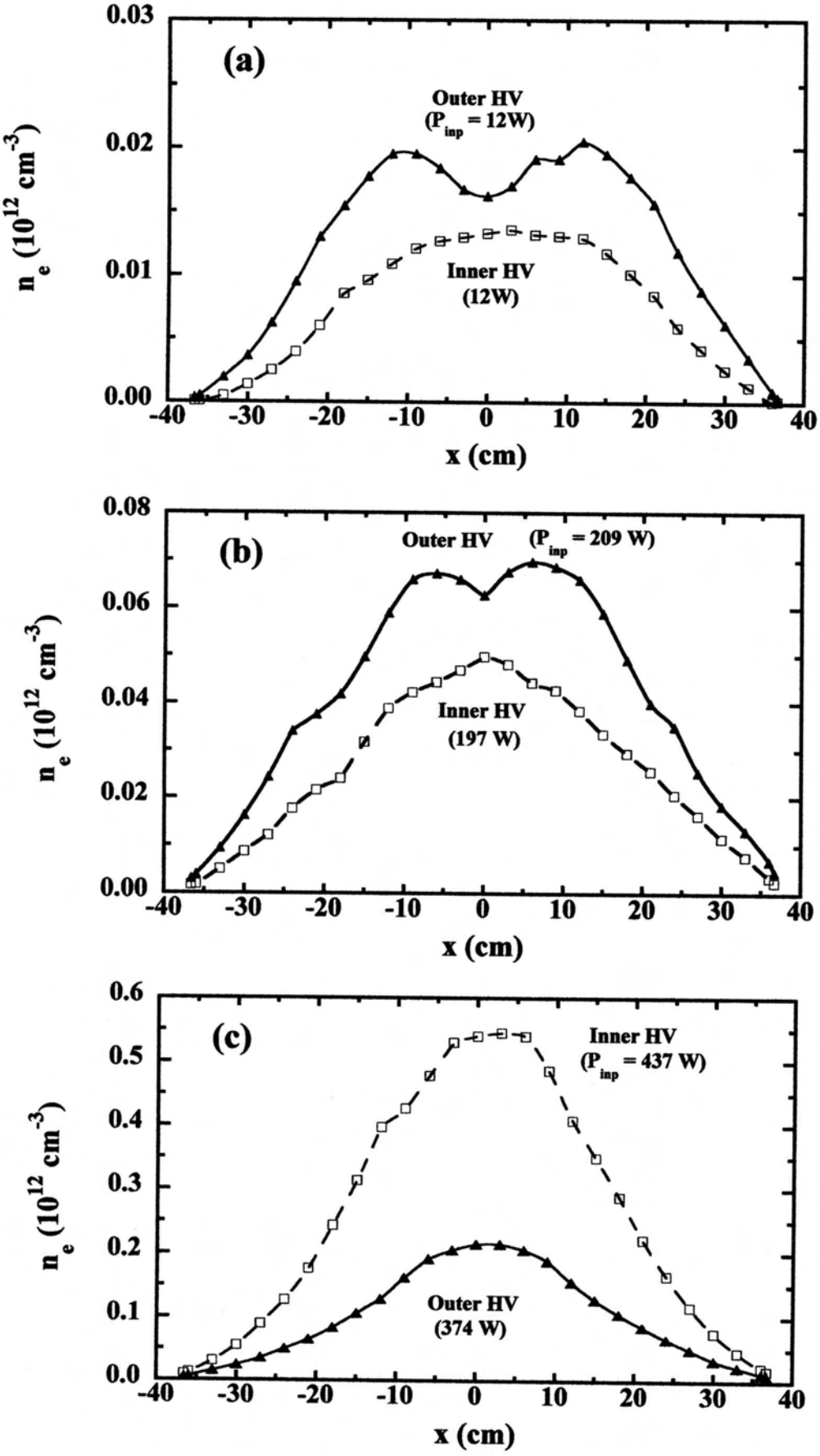

Fig. 11. S. Shirohara et al.

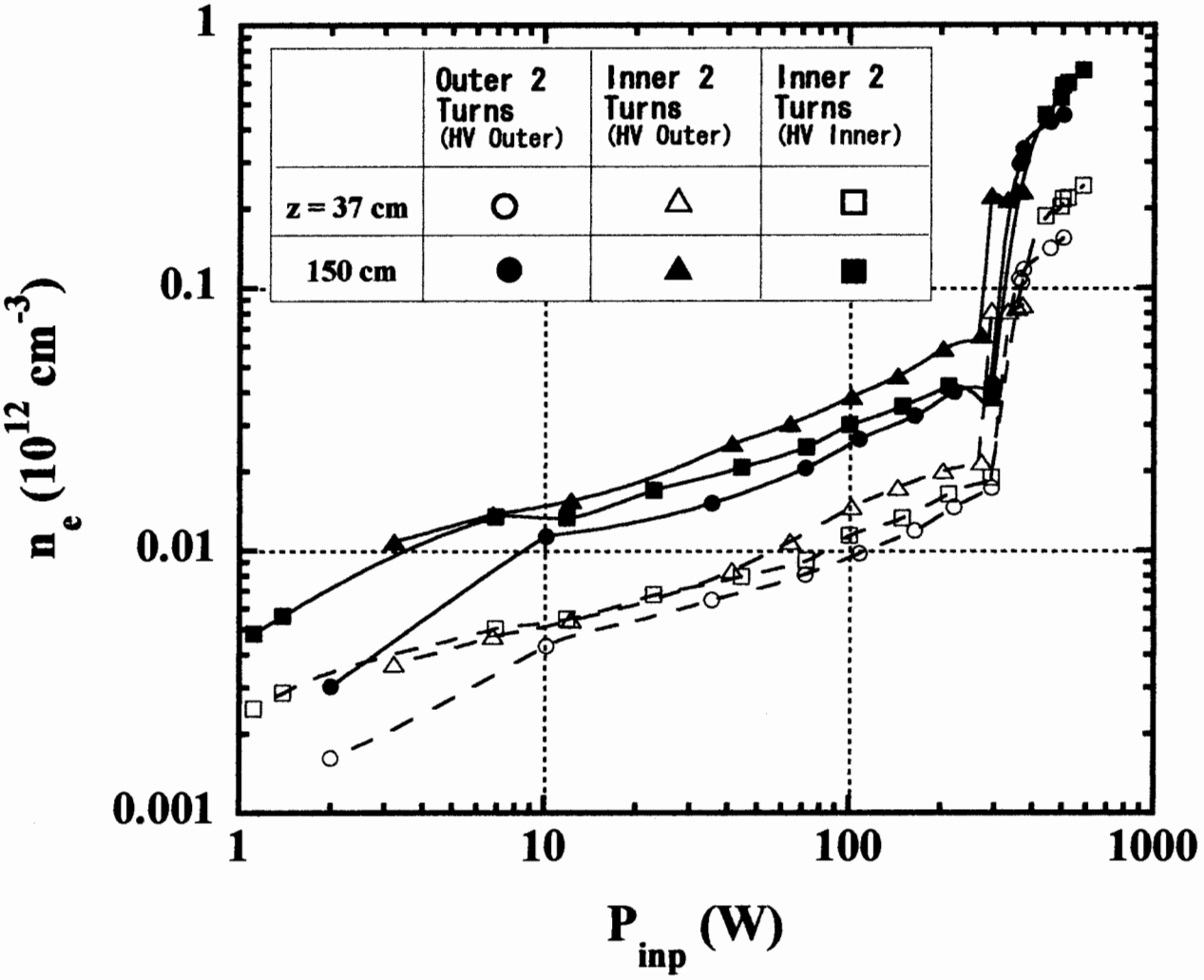

Fig. 12. S. Shinohara et al.

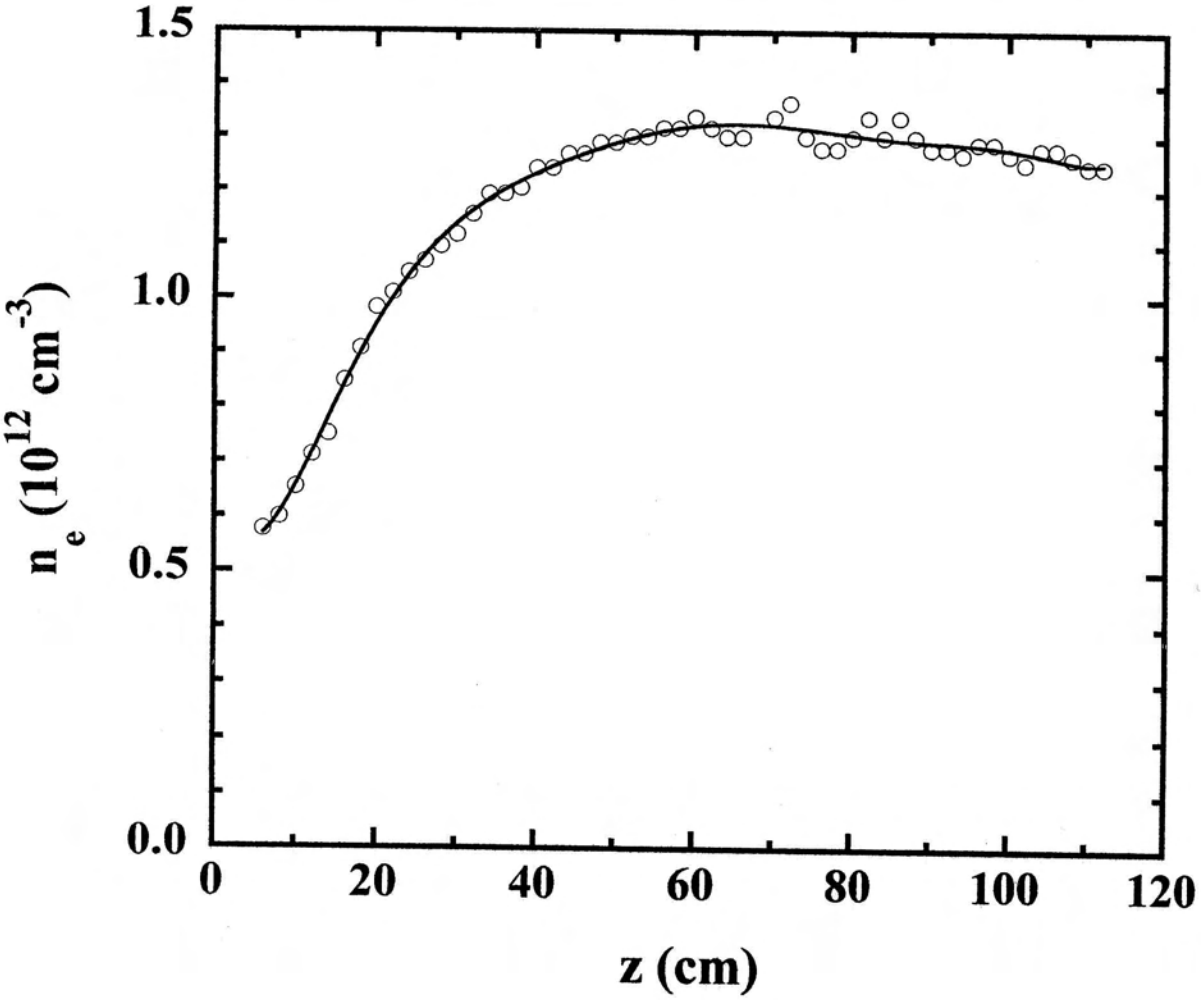

Fig. 13. S. Shinohara et al.

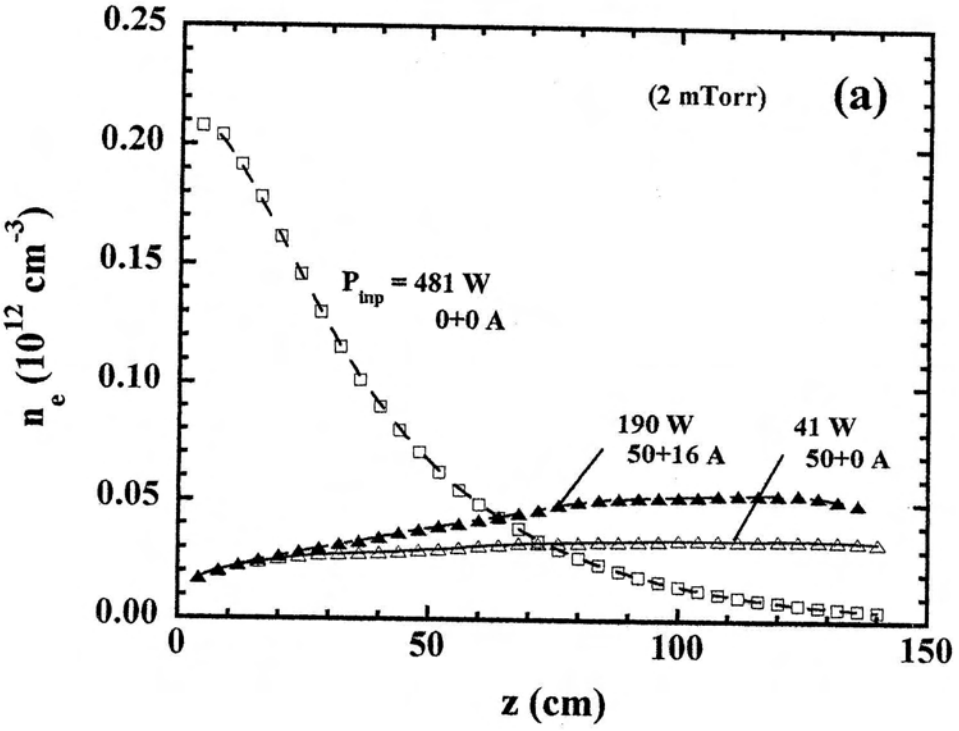

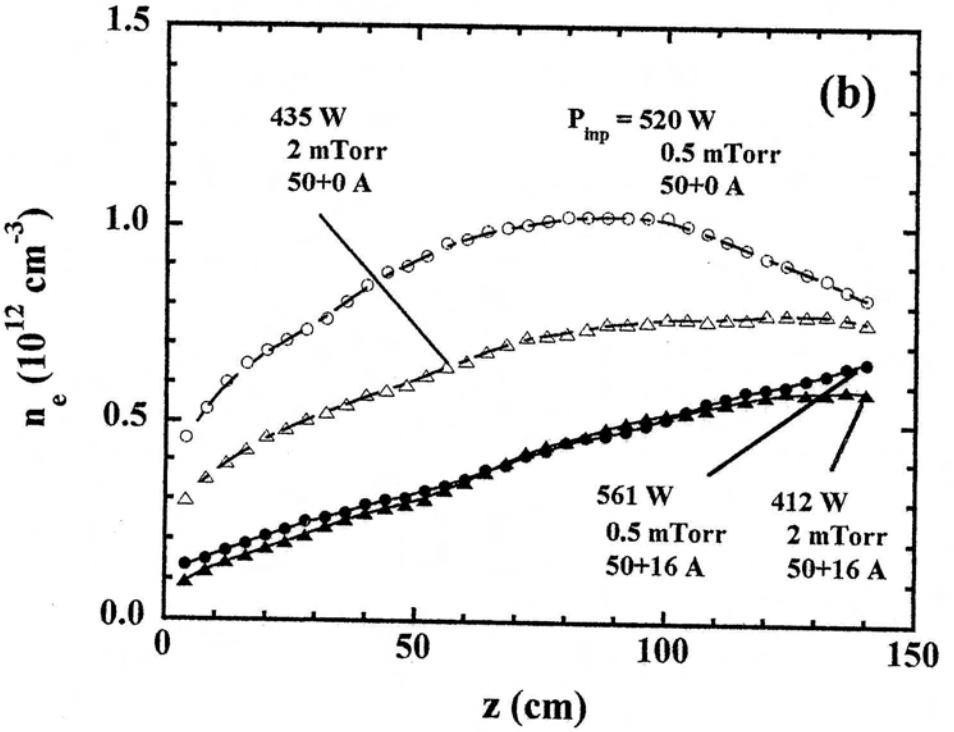

Fig. 14. S. Shinohara et al.